

BIROn - Birkbeck Institutional Research Online

Ziveri, J. and Chhuon, C. and Jamet, A. and Rytter, H. and Prigent, G. and Tros, F. and Barel, M. and Coureuil, M. and Lays, C. and Henry, T. and Keep, Nicholas H. and Guerrera, I.C. and Charbit, A. (2019) Critical role of a sheath phosphorylation site on the assembly and function of an atypical type VI secretion system. *Molecular and Cellular Proteomics* 18 (12), pp. 2418-2432. ISSN 1535-9476.

Downloaded from: <https://eprints.bbk.ac.uk/id/eprint/29301/>

Usage Guidelines:

Please refer to usage guidelines at <https://eprints.bbk.ac.uk/policies.html>
contact lib-eprints@bbk.ac.uk.

or alternatively

Critical role of a sheath phosphorylation site on the assembly and function of an atypical type VI secretion system

Jason Ziveri¹, Cerina Chhuon², Anne Jamet¹, Héloïse Rytter¹, Guénolé Prigent¹, Fabiola Tros¹, Monique Barel¹, Mathieu Coureuil¹, Claire Lays⁴, Thomas Henry⁴, Nicholas H Keep³,
Ida Chiara Guerrero^{2*}, Alain Charbit^{1*}

¹ Université Paris Descartes, Sorbonne Paris Cité, Bâtiment Leriche, Paris, INSERM U1151 - CNRS UMR 8253, Institut Necker-Enfants Malades. Team 11: Pathogenesis of Systemic Infections, Paris, France

² Plateforme protéomique 3P5-Necker, Université Paris Descartes - Structure Fédérative de Recherche Necker, INSERM US24/CNRS UMS3633, Paris 75014, France

³ Crystallography, Institute for Structural and Molecular Biology, Department of Biological Sciences Birkbeck, University of London, United Kingdom

⁴ CIRI, Centre International de Recherche en Infectiologie, Université Lyon, Inserm, U1111, University Claude Bernard Lyon 1, CNRS, UMR5308, École Normale Supérieure de Lyon, Labex Ecofect, Eco-evolutionary dynamics of infectious diseases, F-69007, LYON, France

Running title: *Francisella* sheath phosphorylation and assembly.

Keywords: Type 6 secretion system, Phosphoproteome, *Francisella tularensis*, IgIB.

Bâtiment Leriche. 14 Rue Maria Helena Vieira Da Silva CS 61431 - 75993 PARIS – FRANCE

*Corresponding authors: Ida Chiara Guerrero, Alain Charbit. e-mail:

alain.charbit@inserm.fr; chiara.guerrera@inserm.fr

Tel: 33 1 – 72 60 65 11 — Fax: 33 1 - 72 60 65 13

Abbreviations

T6SS - Type VI secretion system

BMDM - Bone marrow-derived macrophages

CDM - Chemically defined medium

CFU - Colony forming unit

CI - Competition index

DMEM - Dubelcco's modified eagle medium

TiO₂ - Titanium dioxide

Subsp - Subspecies

ASC - Apoptosis-associated speck-like protein containing a CARD

FCP - *Francisella*-containing phagosome

FPI - *Francisella* pathogenicity Island

KEGG - Kyoto encyclopedia of genes and genomes

LAMP - Lysosomal associated membrane protein

LC-MS/MS - Liquid chromatography coupled to tandem mass spectrometry

LFQ - Label free quantification

FDR - False discovery rate

MOI - Multiplicity of infection

OD - Optical density

TSB - Tryptic soy broth

Abstract

The bacterial pathogen *Francisella tularensis* possesses a non-canonical type VI secretion system (T6SS) that is required for phagosomal escape in infected macrophages. KCl stimulation has been previously used to trigger assembly and secretion of the T6SS in culture. By differential proteomics, we found here that the amounts of the T6SS proteins remained unchanged upon KCl stimulation, suggesting involvement of post-translational modifications in T6SS assembly. A phosphoproteomic analysis indeed identified a unique phosphorylation site on IgIB, a key component of the T6SS sheath. Substitutions of Y139 with alanine or phosphomimetics prevented T6SS formation and abolished phagosomal escape whereas substitution with phenylalanine delayed but did not abolish phagosomal escape in J774-1 macrophages. Altogether our data demonstrated that the Y139 site of IgIB plays a critical role in T6SS biogenesis, suggesting that sheath phosphorylation could participate to T6SS dynamics.

Data are available via ProteomeXchange with identifier PXD013619; and on MS-viewer, key lkaqklxwx.

INTRODUCTION

Francisella tularensis is the causative agent of the zoonotic disease tularemia (1-4). Four major subspecies (subsp) of *F. tularensis* are currently listed to cause a fulminant disease in mice that is similar to tularemia in human (5, 6). Although the subsp *novicida* (also called *F. novicida*) is rarely pathogenic in human, its genome shares a high degree of nucleotide sequence conservation with the human pathogenic species and is thus widely used as a model organism (7-9).

This facultative intracellular pathogen is able to infect a variety of different cell types but, *in vivo*, is thought to replicate and disseminate mainly in phagocytes (10). *Francisella* phagosomal escape occurs as early as 30 minutes post-infection (11). A number of factors controlling *Francisella* phagosomal escape and cytosolic multiplication have been already characterized (2, 12-16). Notably, the crucial role of a 30-kb locus in *Francisella* virulence (**Fig. S1**), designated FPI for “Francisella pathogenicity island” (17), has been extensively documented (18). Of note, the FPI is duplicated in three subspecies of *F. tularensis* (subsp *holarctica*, *mediasiatica*, and *tularensis*), but is present in a single copy in *F. novicida* and *F. philomiragia*. The FPI encodes a Type VI secretion system (T6SS) that is essential to promote bacterial phagosomal escape and access to the cytosolic replication niche (19-21). Whereas the transcriptional regulation of the FPI locus has been deeply characterized (22), the molecular mechanisms triggering T6SS assembly and contraction remain largely unknown. Bioinformatic analyses have divided bacterial T6SS in three phylogenetically distinct subtypes (designated T6SSi-iii) (23). Whereas most of the well-characterized T6SS belong to the T6SSi (including in *P. aeruginosa* and *V. cholerae*), *Francisella* is currently the only bacterium to possess a T6SSii (24) known to be exclusively involved in the intracellular life cycle of the pathogen.

The FPI encodes, in addition to the T6SS components, a number of proteins of unknown functions some of which (such as IgIF, PdpC or PdpD) have been proposed or demonstrated to be T6SS effectors (8, 25).

Our current knowledge of the structure and functional assembly of the *Francisella* T6SS are mainly based on recent cryo-electron microscopy data (26, 27) and structural homologies with other members of the T6SSi (26, 27) and references therein). It has been proposed that T6SS resembles a syringe: the tube comprised of IgIC subunits (Hcp homologue) that form hexameric rings fits within the cavity of the IgIA/IgIB sheath (TssB/C in *Pseudomonas*, VipA/B in *Vibrio*), contraction of the sheath results in the ejection of the Hcp tube, together with effector proteins located within the tube and on top of the tip of the tube (28). Formation of the contracted *Francisella* T6SS can be mimicked in vitro by high K⁺ concentration (26). Yet, the molecular relay for this environmental cue remains uncharacterized. In order to understand the mechanisms underlying this KCl-induced T6SS production, we performed a global proteomic analysis on KCl-induced and non-induced bacteria. We found that the relative amounts of most FPI proteins were not increased upon KCl stimulation that suggested the possible implication of a post-translational control of T6SS polymerization. Post-translational modifications (PTMs) constitute a common mechanism that eukaryotic cells employ to polymerize biomolecules. However, in bacteria, polymerization mechanisms are more generally driven by gene expression regulation than by PTMs. Although T6SS sheath polymerization had never been shown to involve any PTM, we hypothesized that protein phosphorylation might occur in *Francisella* and contribute to the dynamics of T6SS assembly-disassembly. By using state-of-the art mass spectrometry analyses, we indeed identified more than one hundred peptides bearing serine/threonine/or tyrosine phosphorylated residues in the proteome of *F. novicida*. One peptide, corresponding to a phosphorylation of IgIB on tyrosine 139 (Y139), particularly attracted our attention. The data presented here reveal that the unique phosphorylatable site of IgIB is essential for the proper activity of this non-canonical T6SS. Functional implications are discussed.

EXPERIMENTAL PROCEDURES

Experimental design and statistical rationale

The (phospho)proteomics data is derived from 3 sets of samples prepared and analyzed by LC-MS/MS for a total of 60 runs performed with 120 min gradient for proteome and 180 min gradient for phosphoproteome measurements on a Q Exactive Plus mass spectrometer. For the proteome data we performed 24 runs for 8 samples (four biological replicates per condition, each run in three technical replicates). For the phosphoproteome data we also performed 24 runs for 8 samples, (four biological replicates per condition, each run in three technical replicates). For the heavy and light sucrose fractions we ran 12 samples in one simple replicate for qualitative analysis. Raw data was processed by MaxQuant software (version 1.5.3.30) as described below. Statistical analysis was performed with Perseus (version 1.6.2.3). For proteome analysis we used t-test, and filtered using $S0=0.5$, $FDR=0.01$ (for class B proteins) and the outer volcano using $S0=0.5$, $FDR=0.001$ (class A proteins). For phosphoproteomics analysis we used t-test $S0=0.1$, $FDR=0.05$. For functional class annotation, COG and EggNog databases were integrated in Perseus. For detailed description of data analysis of each experiment see MS data analysis in the section methods.

For all other experiments: All biological assays were performed in three biological and technical replicates, so that appropriate statistical analysis could be performed. Statistical analysis was performed with two tailed unpaired t-test in GraphPad Prism. P values < 0.05 were considered statistically significant, with * for $p < 0.05$, ** for $p < 0.01$, *** for $p < 0.001$ and **** for $p < 0.0001$. In each experiment, separate controls were included. Images of experiments and western blot were quantified using ImageJ software.

Strains and culture conditions

All strains used in this study are derived from *F. novicida* U112 as described in **Table S1**. Strains were grown at 37°C on pre-made chocolate agar PolyViteX plates (BioMerieux), Schaedler K3 or Chemically Defined Medium (CDM). The CDM used for *F. novicida* corresponds to standard

CDM (29) without threonine and valine (30). For growth condition determination, bacterial strains were inoculated in the appropriate medium at an initial OD₆₀₀ of 0.05 from an overnight culture in Schaedler K3 medium.

T6SS purification

T6SS were prepared essentially as described in (26). Briefly, wild-type *F. novicida* was grown to late exponential phase in Schaedler K3 containing 5% KCl; pelleted by centrifugation and lysed with lysozyme and 1% TritonX-100 detergent in 20 mM Tris HCl, (pH 7.8) with 1 mM EDTA, protease inhibitor cocktail and benzonase nuclease. The lysate was centrifuged 3 times at 15,000 g for 30 min at 4°C to pellet bacterial debris, and the supernatant was layered onto a 10%–55% sucrose gradient overlying a 55% Optiprep cushion and centrifuged at 100,000 g for 18 h. Fractions were collected and examined by transmission electron microscopy (TEM) after negative staining. Briefly, fractions were fixed in 3% paraformaldehyde. Electron microscopy grids were placed on a drop of this suspension and rinsed. The negative contrast was obtained by treating the grids with 2% uranyl acetate for 5 min. The Formvar-coated grids were then observed with a JEOL 1011 transmission electron microscope (tungsten filament) at the Institut Cochin (Paris, France).

The sheath-like structures sedimented to just below the 55% sucrose/Optiprep interface.

Proteomic and Phosphoproteomic analyses

Reagents and chemicals. For protein digestion, dithiothreitol, iodoacetamide and ammonium bicarbonate were purchased from Sigma-Aldrich (St Louis, MO, USA). For phosphopeptide enrichment and LC-MS/MS analysis, trifluoroacetic acid (TFA), formic acid, acetonitrile and HPLC-grade water were purchased from Fisher Scientific (Pittsburgh, PA, USA) at the highest purity grade.

Protein digestion. For proteomic analysis, *F. novicida* was analyzed in three independent biological replicates. Protein concentration was determined by DC assay (Biorad, CA, USA) according to the manufacturer's instructions. An estimated 1.2 mg of proteins for each

biological replicate were digested following a FASP protocol (31) slightly modified. Briefly, proteins were reduced using 100 mM dithiothreitol in 50 mM ammonium bicarbonate for 1h at 60°C. Proteins were then split into four samples of 300 µg and applied on 30 kDa MWCO centrifugal filter units (Microcon, Millipore, Germany, Cat No MRCF0R030). Samples were mixed with 200 µL of 8 M urea in 50 mM ammonium bicarbonate (UA buffer) and centrifuged for 20 min at 15,000 x g. Filters were washed with 200 µL of UA buffer. Proteins were alkylated for 30min by incubation in the dark at room temperature with 100 µL of 50 mM iodoacetamide in UA buffer. Filters were then washed twice with 100 µL of UA buffer (15,000 x g for 15 min) followed by two washes with 100 µL of 50 mM ammonium bicarbonate (15,000 x g for 10 min). Finally, sequencing grade modified trypsin (Promega, WI, USA) was added to digest the proteins in 1:50 ratio for 16 h at 37°C. Peptides were collected by centrifugation at 15,000 x g for 10 min followed by one wash with 50mM ammonium bicarbonate and vacuum dried.

Phosphopeptides enrichment by titanium dioxide (TiO₂) and phosphopeptides purification by graphite carbon (GC). Phosphopeptide enrichment was carried out using a Titansphere TiO₂ Spin tip (3 mg/200 µL, Titansphere PHOS-TiO, GL Sciences Inc, Japan) an estimated 1.2 mg of digested proteins for each biological replicate. Briefly, the TiO₂ Spin tips were conditioned with 20 µL of solution A (80% acetonitrile, 0,1% TFA), centrifuged at 3,000 x g for 2min and equilibrated with 20µL of solution B (75% acetonitrile, 0,075% TFA, 25% lactic acid) followed by centrifugation at 3,000 x g for 2 min. Peptides were resuspended in 10 µL of 2% TFA, mixed with 100 µL of solution B and centrifuged at 1,000 x g for 10min. Sample was applied back to the TiO₂ Spin tips two more times in order to increase the adsorption of the phosphopeptides to the TiO₂. Spin tips were washed with, sequentially, 20 µL of solution B and two times with 20 µL of solution A. Phosphopeptides were eluted by the sequential addition of 50 µL of 5% NH₄OH and 50 µL of 5% pyrrolidine. Centrifugation was carried out at 1,000 x g for 5 min.

Phosphopeptides were further purified using GC Spin tips (GL-Tip, Titansphere, GL Sciences Inc, Japan). Briefly, the GC Spin tips were conditioned with 20 µL of solution A, centrifuged

at 3,000 x g for 2 min and equilibrated with 20 μ L of solution C (0,1% TFA in HPLC-grade water) followed by centrifugation at 3,000 x g for 2 min. Eluted phosphopeptides from the TiO₂ Spin tips were added to the GC Spin tips and centrifuged at 1,000 x g for 5 min. GC Spin tips were washed with 20 μ L of solution C. Phosphopeptides were eluted with 70 μ L of solution A (1,000 x g for 3 min) and vacuum dried.

nanoLC-MS/MS protein identification and quantification. Samples were resuspended in 12 μ L of 0.1% TFA in HPLC-grade water. For each run, 5 μ L was injected in a nanoRSLC-Q Exactive PLUS (RSLC Ultimate 3000, Thermo Scientific, MA, USA). Phosphopeptides were loaded onto a μ -precolumn (Acclaim PepMap 100 C18, cartridge, 300 μ m i.d.x5 mm, 5 μ m, Thermo Scientific, MA, USA) and were separated on a 50 cm reversed-phase liquid chromatographic column (0.075 mm ID, Acclaim PepMap 100, C18, 2 μ m, Thermo Scientific, MA, USA). Chromatography solvents were (A) 0.1% formic acid in water, and (B) 80% acetonitrile, 0.08% formic acid. Phosphopeptides were eluted from the column with the following gradient 5% to 40% B (180 min), 40% to 80% (6 min). At 181 min, the gradient returned to 5% to re-equilibrate the column for 20 minutes before the next injection. Two blanks were run between each sample to prevent sample carryover.

Phosphopeptides eluting from the column were analyzed by data dependent MS/MS, using top-8 acquisition method. Phosphopeptides were fragmented using higher-energy collisional dissociation (HCD). Briefly, the instrument settings were as follows: resolution was set to 70,000 for MS scans and 17,500 for the data dependent MS/MS scans in order to increase speed. The MS AGC target was set to 1×10^6 counts with maximum injection time set to 250 ms, while MS/MS AGC target was set to 2×10^5 with maximum injection time set to 250 ms. The MS scan range was from 400 to 1.800 m/z. MS and MS/MS scans were recorded in profile mode. Dynamic exclusion was set to 30 seconds.

For proteomic analysis, peptides were eluted from the column with the following gradient 5% to 40% B (120 min), 40% to 80% (6 min). At 127 min, the gradient returned to 5% to reequilibrate the column for 20 min before the next injection. Peptides eluting from the column were analyzed by data dependent MS/MS, using the top-10 acquisition method. Peptides were

fragmented using higher-energy collisional dissociation (HCD). Briefly, the instrument settings were as follows: resolution was set to 70,000 for MS scans and 17,500 for the data dependent MS/MS scans in order to increase speed. The MS AGC target was set to 3.106 counts with maximum injection time set to 60 ms, while MS/MS AGC target was set to 1.105 with maximum injection time set to 60 ms. The MS scan range was from 400 to 2000 m/z. Dynamic exclusion was set to 30 sec duration.

Data Processing Following nanoLC-MS/MS acquisition. The MS files were processed with the MaxQuant software version 1.5.3.30 and searched with Andromeda search engine against the UniProtKB/Swiss-Prot *F. novicida* database (release 28-04-2014, 1719 entries). To search parent mass and fragment ions, we set an initial mass deviation of 4.5 ppm and 0.5 Da respectively. The minimum peptide length was set to 7 amino acids and strict specificity for trypsin cleavage was required, allowing up to two missed cleavage sites. Carbamidomethylation (Cys) was set as fixed modification, whereas oxidation (Met), N-term acetylation and phosphorylation (Ser, Thr, Tyr) were set as variable modifications (only for phosphoproteomics analysis). The match between runs option was enabled with a match time window of 0.7 min and an alignment time window of 20 min. The false discovery rates (FDRs) at the protein and peptide level were set to 1%. Scores were calculated in MaxQuant as described previously (32). The reverse and common contaminants hits were removed from MaxQuant output.

The phosphopeptides output table and the corresponding logarithmic intensities were used for phosphopeptide analysis. The phosphopeptide table was expanded to separate individual phosphosites, and we kept all sites identified in at least three out of four replicates in at least one group (no KCl vs KCl). Missing values were imputed using width=0.2 and down-shift=3. We represented on a heatmap the significantly altered phosphosites (t-test $S_0=0.1$, FDR=0.05).

The proteingroups output table was used for total proteome analysis, we kept only proteins identified in all four replicates in at least one group (noKCl vs KCl). Missing values were imputed using width=0.3 and down-shift=2.5. For volcano plot we used t-test, $S_0=0.5$,

FDR=0.01 (for class B proteins) and the outer volcano using $S_0=0.5$, FDR=0.001 (class A proteins).

Construction of a $\Delta iglB$ deletion mutant

We inactivated the gene *iglB* in *F. novicida* (FTN_1323) by allelic replacement, resulting in the deletion of the entire gene (4 first codons and 7 last codons were conserved). We constructed a recombinant PCR product containing the upstream region of the gene *iglB* (*iglB*-UP), a kanamycin resistance cassette (*nptII* gene fused with *pGro* promoter) and the downstream region of the gene *iglB* (*iglB*-DN) by overlap PCR. Primers *iglB* upstream FW (p1) and *iglB* upstream (spl_K7) RV (p2) amplified the 689 bp region upstream of position +3 of the *iglB* coding sequence (*iglB*-UP), primers *pGro* FW (p3) and *nptII* RV (p4) amplified the 1091 bp kanamycin resistance cassette (*nptII* gene fused with *pGro* promoter); and primers *iglB* downstream (spl_K7) FW (p5) and *iglB* downstream RV (p6) amplified the 622 bp region downstream of the position +1520 of the *iglB* gene coding sequence (*iglB*-DN). Primers p2 and p5 have an overlapping sequence of 12 nucleotides with primers p3 and p4 respectively resulting in fusion of *iglB*-UP and *iglB*-DN with the cassette after cross-over PCR (**Table S2**). All single fragment PCR reactions were realized using Phusion High-Fidelity DNA Polymerase (ThermoScientific) and PCR products were purified using NucleoSpin® Gel and PCR Clean-up kit (Macherey-Nagel). Overlap PCRs were carried out using 100 ng of each purified PCR products and the resulting fragment of interest was purified from agarose gel. This fragment was then directly used to transform wild type *F. novicida* by chemical transformation (30). Recombinant bacteria were isolated on Chocolate agar plates containing kanamycin ($10 \mu\text{g mL}^{-1}$). The mutant strains were checked for loss of the wild type gene by PCR product direct sequencing (GATC-biotech) using appropriate primers.

Functional complementation

The $\Delta iglB$ mutant strain was transformed with the recombinant pKK214-derived plasmids (pKK-*iglBY139A_{cp}*, pKK-*iglBY139F_{cp}*, pKK-*iglBY139D_{cp}* and pKK-*iglBY139E_{cp}*) described below (**Table S1**). Primers pGroFW and pGro RV amplified the 328 bp of the *pGro* promoter;

primers *iglB* FW/ and *iglB*[PstI] RV amplified the 1,534 bp *iglB* gene from U112. PCR products were purified and *Sma*I (*pGro* promoter) or *Pst*I (*iglB*) digested in presence of FastAP Thermosensitive Alkaline Phosphatase (ThermoScientific) to avoid self-ligation. Mixtures of *pGro* promoter and fragments of the genes of interest were then incubated with T4 DNA Ligase (New England Biolabs) to allow blunt end ligation and fragments were then cloned in pKK214 vector after *Sma*I/*Pst*I double digest and transformed in *E. coli* TOP10. Recombinant plasmid pKK-*iglB*_{cp} was purified and directly used for chemical transformation in *F. novicida* Δ *iglB* (30). Recombinant colonies were selected on Chocolate agar plates containing tetracycline (5 μ g mL⁻¹) and kanamycin (10 μ g mL⁻¹).

For site-directed mutagenesis of *iglB* gene, we used plasmid pKK-*iglB*_{cp}. The recombinant plasmids pKK-*iglBY139A*_{cp}, pKK-*iglBY139F*_{cp}, pKK-*iglBY139D*_{cp} and pKK-*iglBY139E*_{cp} were constructed using the primer pairs *iglB* (Y/A, Y/F, Y/D, or Y/E) FW and *iglB* RV (**Table S2**).

The three first bases of primers *iglB* FW were modified to change Tyr139 to Ala, Phe, Asp or Glu. PCR products were purified, phosphorylated by the T4 Polynucleotide Kinase and then incubated with T4 DNA Ligase (New England Biolabs) and transformed in *E. coli* TOP10. Recombinant plasmids were purified and directly used for chemical transformation in *F. novicida* Δ *iglB*, as described previously (30). Recombinant colonies were selected on Chocolate agar plates containing tetracycline (5 μ g mL⁻¹) and kanamycin (10 μ g mL⁻¹).

Gfp-expressing F. novicida

The Δ *iglB* mutant strain was transformed with the recombinant plasmids pKK-GFP-*iglBWT*_{cp} and pKK-GFP-*iglBY139F*_{cp}, derived from pKK214-GFP (33). Primers *pGroFW* and *iglBRV* (**Table S2**) amplified the 1,870 bp of the *pGro-iglB* from the pKK-*iglBWT*_{cp} and pKK-*iglBY139F*_{cp}. PCR products were purified and digested with *Sma*I and the *pGro-iglB WT* and *pGro-iglB Y139F* fragments were then incubated with T4 DNA Ligase (New England Biolabs) to allow blunt end ligation and fragments were then cloned in the unique *Sma*I site of pKK214-(GFP) vector and transformed in *E. coli* TOP10. Recombinant plasmid pKK-(GFP)-*iglBWT*_{cp} and pKK-(GFP)-*iglBY139F*_{cp} were purified and directly used for chemical

transformation in *F. novicida* $\Delta iglB$ (30). Recombinant colonies were selected on Chocolate agar plates containing tetracycline (5 $\mu\text{g mL}^{-1}$) and kanamycin (10 $\mu\text{g mL}^{-1}$).

Immunodetection

Antibodies to IglA, IglB and IglC were obtained through the NIH Biodefense and Emerging Infections (BEI) Research Resources Repository, NIAID, NIH.

Immunoblotting analysis. Protein lysates for immunoblotting were prepared by using Laemmli sample buffer. Protein lysates corresponding to equal OD₆₀₀ were loaded on 12% Bis/Tris gels (Invitrogen), and run in TGS buffer. Primary antibodies (anti-IglA or anti-IglB) were used at final dilution of 1:2,000. Secondary horseradish peroxidase (HRP)-conjugated goat antimouse antibody (Santa Cruz Biotechnology, CA, USA) or (HRP)-conjugated goat anti-rabbit antibody and the enhanced Chemiluminescence system (ECL) (Amersham Biosciences, Uppsala, Sweden) were used as previously described (34).

Co-immunoprecipitations. Wild-type *F. novicida* was grown to late exponential phase in Schaedler K3; collected by centrifugation and lysed with lysozyme and 1% TritonX-100 detergent in 20 mM Tris HCl, (pH 7.8) with 1 mM EDTA, protease inhibitor cocktail and benzonase nuclease. The lysate was centrifuged at 15,000 g for 15 min at 4°C to pellet bacterial debris. Monoclonal anti-IglB antibody was incubated 40 min with Dynabeads protein G (Invitrogen) and the complex was incubated at room temperature with the bacterial lysate for 1 hour. After washing, the complex was loaded on 12% Bis/Tris gels (Invitrogen), and run in TGS buffer.

Cell cultures and cell infection experiments

J774A.1 (ATCC® TIB-67™) cells were propagated in Dulbecco's Modified Eagle's Medium (DMEM, PAA), containing 10% fetal bovine serum (FBS, PAA) unless otherwise stated. The day before infection, approximately 2×10^5 eukaryotic cells per well were seeded in 12-well cell tissue plates and bacterial strains were grown overnight in 5 mL of Schaedler K3 at 37°C. Infections were realized at a multiplicity of infection (MOI) of 100 and incubated for 1 h

at 37°C in culture medium. After 3 washes with cellular culture medium, plates were incubated for 4, 10 and 24 h in fresh medium supplemented with gentamycin (10 µg mL⁻¹). At each kinetic point, cells were washed 3 times with culture medium and lysed by addition of 1 mL of distilled water for 10 min at 4°C. The titer of viable bacteria was determined by spreading preparations on chocolate plates. Each experiment was conducted at least twice in triplicates.

Time lapse microscopy

J774-1 cells were transduced with the IncuCyte® NucLight Red Lentivirus, following the manufacturer's recommendations, to obtain red nuclear labelling of living cells due to the expression of the red fluorescent protein mKate2 containing a nuclear localization signal. One prior to infection, J774-1 cells were seeded in 12-well cell tissue plates. Cells were infected (MOI of 1,000) with wild-type and mutant GFP-expressing cell. Synchronization of bacterial entry was realized by a 5 minutes centrifugation at 1,000 rpm. Plates were then incubated for 1 h at 37°C in culture medium. After 3 washes with cellular culture medium, plates were incubated at 5% CO₂ and 37°C for 24 hours in fresh medium supplemented with gentamycin (10 µg mL⁻¹). Bacterial multiplication was monitored in the fully automated microscope Incucyte® S3 (Essen BioScience). Images were taken every 20 minutes with the 20X objective. Analysis and time-lapse videos (from which images were extracted) were generated by using Incucyte® S3 software.

Confocal microscopy experiments

J774.1 macrophage cells were infected (MOI of 1,000) with wild-type *F. novicida* U112, the isogenic '*iglB*' mutant, the '*iglB*' complemented either with wild-type *iglB* (CpWT) Y139A, Y139F mutants or an isogenic '*FPI*' strain, in standard DMEM (DMEM-glucose) for 30 min at 37°C. Cells were then washed three times with PBS and maintained in fresh DMEM supplemented with gentamycin (10 Pg mL⁻¹) until the end of the experiment. Three kinetic points (*i.e.* 1 h, 4 h and 10 h) were sampled. For each time point, cells were washed with 1X

PBS, fixed 15 min with 4% paraformaldehyde, and incubated 10 min in 50 mM NH₄Cl in 1X PBS to quench free aldehydes. Cells were then blocked and permeabilized with PBS containing 0.1% saponin and 5% goat serum for 10 min at room temperature. Cells were then incubated for 30 min with anti-*F. novicida* mouse monoclonal antibody (1/500e final dilution, Creative Diagnostics) and anti-LAMP1 rabbit polyclonal antibody (1/100e, ABCAM). After washing, cells were incubated for 30 min with Alexa488-conjugated goat anti mouse and Alexa546 conjugated donkey anti rabbit secondary antibodies (1/400e, AbCam). After washing, DAPI was added (1/1,000) for 1 min and glass coverslips were mounted in Mowiol (Cityfluor Ltd.). Cells were examined using an X63 oil-immersion objective on a Zeiss Apotome 2 microscope. Co-localization tests were quantified by using Image J software; and mean numbers were calculated on more than 500 cells for each condition. Confocal microscopy analyses were performed at the Cell Imaging Facility (Faculté de Médecine Necker Enfants-Malades).

Transmission electron microscopy experiments

J774.1 macrophages were grown and infected at an MOI of 1,000 with wild-type *F. novicida* U112, or the isogenic *igIB* mutants Y139A, Y139F mutants, in standard DMEM (DMEMglucose) for 30 min at 37°C (as described above). 24 h after infection, infected cells were fixed with glutaraldehyde 3% in phosphate buffer during one hour. Cells were then post-fixed with osmium tetroxide to stabilize lipids and enhance contrast. Samples were then dehydrated with sequential ethanol baths (from 25% to 100%) and embedded in Epon 812 resin with a 48 hours polymerization time at 60°C. Embedded samples were sliced in 90 nm thick pieces with an ultramicrotome and laid down on a copper observation grid. Image acquisitions were performed with a JEOL 1011 transmission electron microscope (tungsten filament) at the Institut Cochin (Paris, France).

BMDMs Infections

Infection of WT or *ASC^{-/-}* bone marrow-derived macrophages (BMDMs) was performed as described previously (35). Briefly, BMDMs were differentiated in DMEM (Invitrogen) with 10%

v/v FCS (Thermo Fisher Scientific), 15% MCSF (L929 cell supernatant), 10 mM HEPES (Invitrogen), and non-essential amino acids (Invitrogen). One day before infection, macrophages were seeded into 12- 48- or 96-well plates at a density of 2×10^5 , 1.5×10^5 or 5×10^4 cells per well, respectively and incubated at 37°C, 5% CO₂. The overnight culture of bacteria was added to the macrophages at multiplicity of infection (MOI) of 100. The plates were centrifuged for 15 min at 500 x g to ensure comparable adhesion of the bacteria to the cells and placed at 37°C for 1h. After 3 washes with PBS, fresh medium with 5 µg mL⁻¹ gentamycin (Invitrogen) was added to kill extracellular bacteria and plates were incubated for the desired time.

Phagosomal rupture assay

Quantification of vacuolar escape using the β-lactamase/CCF4 assay (Life technologies) was performed as previously described (36). ASC^{-/-} BMDMs seeded onto non-treated plates were infected as described above for 2 h, washed and incubated in CCF4 for 1 h at room temperature in the presence of 2.5 mM probenidicid (Sigma). Propidium iodide negative cells were considered for the quantification of cells containing cytosolic *F. novicida* using excitation at 405 nm and detection at 450 nm (cleaved CCF4) or 510 nm (intact CCF4).

Sequence analyses

To retrieve IgIB homologous proteins, we used the Hidden Markov Model (HMM) profile “T6SSii_igIB.hmm” from reference (24). We scanned a dataset of 2,462 predicted proteomes of complete bacterial genomes retrieved from GenBank Refseq (last accessed September 2016) using *hmmsearch* program of HMMER v.3.1b2 (gathering threshold = 25).

Our dataset included 19 genomes of the *Francisella* genus. All IgIB sequences encoded by *Francisella* genomes were aligned with MUSCLE v.3.8.31 (37). Due to differences in the annotation of the first methionine codon, we used the sequence of FTN_1323 as a reference for the multiple sequence alignment.

Redundancy of the sequence set retrieved from *hmmsearch* was reduced using *cd-hitv4.6.7* (38) with a 90% identity threshold. The longest representative sequence of each cluster was then aligned with *MUSCLE v.3.8.31* (37). Outliers that were very divergent in sequence length were removed. *PROMALS3D* and *ESPrpt3.0* (39) servers were used to visualize multiple sequence and structure alignment using *3J9O.B* PDB structure reference file (26). To determine the conservation of the phosphotyrosine site identified in *Francisella* genus (Tyr139 or Y139) we focused on the 12 amino acids surrounding the *Francisella* Tyr139 residue in the 535 aligned sequences.

To determine the conservation of the phosphotyrosine site identified in *Francisella* genus (Tyr139) we focused on the 12 amino acids surrounding the *Francisella* Y139 residue in the 535 aligned sequences. Out of the 535 aligned sequences, we found 90 sequences with a tyrosine residue in the vicinity of *Francisella* Tyr139 residue. For illustrative purpose, we selected 12 representative sequences out of 90 as shown in **Fig. S3**.

Data Availability

The mass spectrometry proteomics data have been deposited to the ProteomeXchange Consortium via the PRIDE (40) partner repository with the dataset identifier PXD013619.

RESULTS

We first monitored sheath formation upon KCl stimulation, using the procedure previously described (26). Briefly, lysates of wild-type *F. novicida*, grown in the presence of 5% KC, were layered onto 15%-55% sucrose gradients (**Fig. 1A**). The fraction sedimenting in equilibrium at 55% sucrose and below (55% Optiprep, grey arrow) from KCl-induced cultures were further dialyzed and used for negative staining TEM imaging. As expected, rod-shaped particles were detected by transmission electron microscopy in this fraction that corresponded to contracted sheath-like structures (**Fig. 1A and Fig S2**). In contrast, we failed to visualize such structures in any of the other fractions of the gradient tested. The different fractions of the gradient were next tested by western blotting with anti-IglA and anti-IglB antibodies. IglA and IglB were detected in all the fraction of the gradient in KCl-induced conditions (**Fig. 1B**). Since KCl induction is required to trigger sheath polymerization, we anticipated that IglA and IglB would not be detected in the lower fractions of the gradient in non KCl-induced conditions. Indeed, in the absence of KCl induction, the two proteins were only detected in the fractions of the upper half of the gradient (in the 15% and in part of the 35% sucrose fractions). We next decided to perform a whole cell proteome analysis of KCl-induced and non-induced bacterial cultures.

Whole cell proteome analyses

Whole cell extracts from KCl-induced and non-induced cultures were analyzed in order to identify proteins whose abundance was altered by the KCl treatment. We could quantify 1,395 proteins that represent 80% of the predicted *Francisella* proteome (**Table S3**). Upon KCl stimulation, 113 proteins were up-regulated after KCl stimulation and 97 down-regulated, confirming that KCl stimulation strongly alters the proteome of the cell (**Table S3, Fig. 1C**). Remarkably, the amounts of most of the FPI-encoded proteins (17 out the 18 proteins encoded by the FPI were identified) did not change significantly upon KCl stimulation, including notably the sheath and tube proteins IglA, IglB, IglC (blue dots in **Fig. 1C**). The down-regulated proteins

included seven proteins (FTN_0042 to FTN_0048) encoded by the “*Francisella novicida* island” (or FNI), a genomic island that shows some similarities with the FPI (35), where FTN_0042 and FTN_0043 correspond to the orthologues of IglA and IglB, respectively). Oppositely, two sets of proteins emerged as up-regulated (**Fig. S3A**): proteins involved in Iron-sulfur (Fe/S) clusters biogenesis (FTN_0751 to FTN_0754, FTN_0850 to FTN_0853 and FTN1082) as well as most of the protein encoded by the *fig* (also designated *fsI*) operon (41, 42), involved in iron acquisition (FTN_1681, FTN_1682, FTN_1684 to FTN_1687) (**Fig. S3B**). On the basis of the known regulation of Fe/S clusters in other bacterial species (43, 44), these Fe/S cluster proteins could be regulated by FTN_0810, a predicted transcriptional regulator sharing modest sequence identity with the Fe/S regulator IscR.

The fact that the amounts of T6SS proteins remained unchanged upon KCl induction, led up to hypothesize that a post-translational mechanism might be responsible for KCl-dependent sheath polymerization.

The phosphoproteome of Francisella

Our careful inspection of the *Francisella* genomes did not identify any gene encoding for a putative serine/threonine-protein kinase or tyrosine kinase. In spite of this lack of canonical kinases, we hypothesized that serine/threonine/tyrosine phosphorylation of proteins might occur in *Francisella* and contribute to pathogenesis. We therefore carried out a global and site-specific phosphoproteomic analysis of *F. novicida* (strain U112), based on phosphopeptide enrichment and high-resolution LC-MS/MS analysis from KCl-induced and non-induced cultures (**Fig. 2**). Overall, this analysis allowed the identification of 103 phosphopeptides, of which 78 were robustly quantified. The majority of the phosphosites (47 out of 78) were found on serine residues (S), while similar lower number of sites, 19 and 12, were found on threonine (T) and tyrosine (Y), respectively (**Fig. 2A, B; Table S4**). These phosphosites corresponded to 59 proteins, of which 7 presented multiple phosphorylation sites. These proteins belonged

to various functional categories and the most represented classes were carbohydrate metabolism, energy production and conversion and translation.

IglB was the only protein of the T6SS that we found to be phosphorylated on Y139, particularly after KCl stimulation (**Fig. 2C**). As mentioned above, IglB constitutes with IglA the T6SS sheath of *Francisella* (17, 26, 35).

Y139 is a conserved amino acid

Comparative sequence analyses on 33 IglB proteins from 19 genomes of the *Francisella* genus were performed to assess the conservation of residue Tyr139 (**Fig. S4**). Sequences were highly conserved between 31 IglB proteins sharing 93 to 100% amino acid identity. In contrast, the proteins encoded by *FTN_0043* in the FNI (35) and *F7308_1917* (*Fsp_TX077308*) exhibited only 48% amino acid identity with the 31 other IglB proteins whereas they both share 85% identity. Excluding these 2 outliers, among 506 sites, 458 were without polymorphism (91%), with Tyr139 conserved in all IglB sequences (**Fig. S4**, upper part). Since IglB is among the most conserved components of T6SS (17, 26), we were able to retrieve orthologues of IglB encoded outside of *Francisella* genus. Out of 535 nonredundant IglB orthologues (also named VipB, TssC or EvpB/VC_A0108), we found 90 sequences with a tyrosine in the vicinity of Tyr139 site outside of *Francisella* genus. In 82 sequences, the predicted location of the tyrosine residue was similar to that of Tyr139 (in a turn region between two helices) (**Fig. S4**, lower part).

IglB phosphorylation in sheath formation

In order to determine if the phosphorylated forms of IglB was incorporated into the sheath upon its assembly, we further compared the phosphoprotein content of the fractions at the bottom of the gradient (sucrose 55%-Optiprep 55% density zone), containing the sheath-like particles, to the fractions at the top of the gradient (15-35% sucrose density zone), presumably containing non-polymerized forms of the IglA and IglB proteins (hereafter called “heavy fraction”, H or “light fraction”, L, respectively) (**Fig. 2D, Table S5**).

The mass spectrometry analysis of the H and L fractions identified over 1,145 proteins (**Table S6**) and confirmed the efficiency of the sucrose gradient separation. Unmodified peptides

containing Tyr139 were detected in both H and L fractions, indicating that soluble IgIB include both phosphorylated and non-phosphorylated forms of the protein. Importantly, the peptide bearing the phosphorylated tyrosine residue (pY139) of IgIB was only detected in the L fraction of the gradient (**Table S5**), suggesting that tyrosine phosphorylation might be unfavorable for sheath polymerization.

Fully supporting this notion, our 3D predictions (**Fig. 3**) indicate that, upon addition of a phosphoryl moiety at this position, charge repulsion between the phosphate group and nearby aspartate residues should be unfavorable for the formation of stable hexameric rings and sheath contraction. Since the phosphate on Y139 is linked to the O⁴ position of the phenolic ring, the effects of Tyr phosphorylation may be exerted primarily through allosteric/electrostatic effects. Looking at the full helical reconstruction, one can see that Y139 is close to both D63 of IgIA and D114 of IgIB. These are from two different symmetryrelated chains (**Fig. 3**). Putting a phosphate on Y139 is thus likely to repel the aspartate residues and to disassemble the structure.

Functional assays to understand the role of phosphorylation on Y139.

We hereafter thoroughly evaluated the importance of Y139 phosphorylation on T6SS functionality and *Francisella* pathogenicity. For this, we constructed two IgIB variants in which Tyr139 was substituted either by an alanine (A) or by the non-phosphorylatable aromatic amino acid analogue of tyrosine, phenylalanine (F). These IgIB mutated proteins (designated Y139A and Y139F, respectively) were expressed *in trans* in a Δ igIB mutant of *F. novicida* carrying a chromosomal deletion of the entire *igIB* gene, (see Materials and Methods). A mutant with a deletion of the entire *FPI* (Δ FPI) and a Δ igIB deletion mutant were used as negative controls. Both mutants are unable to escape from phagosomes and hence to grow in macrophages (45). IgIB was detected by Western blotting on whole cell lysates in wild-type and complemented mutated strains (Y139A and Y139F) but not in the Δ igIB and Δ FPI strains (**Fig. 4A**). IgIA was also detected in wild-type and complemented mutated strains (Y139A and Y139F), but in lower amounts in the Δ igIB strain and not in the Δ FPI mutant. This observation is in agreement

with earlier observations (46) that suggested that the presence of IgIB increases the stability of IgIA.

A classical measure of basal T6SS function is the export of an Hcp-related protein (IgIC in *F. novicida*). Therefore, we examined IgIB-dependent IgIC export in the different *F. novicida* mutant strains by Western-blot on bacteria grown in the presence -or absence- of 5% KCl. In agreement with previous reports, IgIC was detected in the culture supernatant in the presence, but not in the absence, of KCl, in the wild-type and *igIB*_{WT} complemented strains. In contrast, deletion of *igIB* as well as the two single amino acid substitutions Y139A and Y139F, all abolished the secretion of IgIC into the culture medium (**Fig. 4B**, right). We also verified that it is due to secretion impairment as KCl treatment did not modify the amounts of IgIA, IgIB and IgIC proteins detected by western blotting on whole cells (bacterial pellet fractions) (Fig 4b, left). These results confirmed the proteomics data (Fig 1C).

To check the impact of the two amino acid substitutions on IgIA-IgIB heterodimer formation, we performed co-immunoprecipitation assays (**Fig. 4C**). We used either anti-IgIA to precipitate the complex, followed by western blotting with anti-IgIB (upper panel) or anti-IgIB, followed by western blotting with anti-IgIA (lower panel). In both conditions, the two IgIB mutants were still able to interact with IgIA to form IgIA-IgIB heterodimers.

We next performed sucrose gradient fractionation (as described above), followed by western blotting with anti-IgIB on the Y139F and Y139A mutant strains. The Y139F IgIB mutant protein was detected in both the L and H fractions of the gradient (**Fig. 4D**), indicating that some sheath polymerization still occurred in the Y139F mutant. In contrast, the Y139A mutant protein was detected in the upper fractions of the gradient but not in the lower fractions (corresponding to the contracted sheath). Fully supporting the western-blot data, proteomic analysis of the distribution of IgIA and IgIB in the Heavy (H) and light (L) sucrose fraction revealed that their distribution was similar in the strains expressing either WT IgIB and Y139F IgIB with, in both case, a slightly higher proportion of IgIA and IgIB in the L fraction compared to the H fraction. In sharp contrast, with the Y139A mutant, IgIB was absent from the H fraction and IgIA also almost exclusively found in the L fraction (**Fig. 4E**;

Table S6).

Critical role of residue Y139 in Francisella pathogenesis

The mutations Y139A and Y139F had no effect on bacterial growth in broth (**Fig. S5**). We therefore decided to verify the ability of wild-type *F. novicida* (WT), $\Delta iglB$ and complemented strains (CpWT, Y139A and Y139F) to survive and multiply in murine macrophage-like J774.1 cells over a 24 h-period (**Fig. 5A**). Confirming earlier reports (47), intracellular multiplication of the $\Delta iglB$ mutant was essentially abolished and comparable to that of the ΔFPI mutant. The single amino acid substitution of Y139 by an alanine (Y139A) also abolished intracellular bacterial multiplication. In contrast, when Y139 was substituted by a phenylalanine (Y139F), although cytosolic growth was prevented until 10 h after infection, at 24 h the Y139F mutant strain had actively multiplied (ultimately leading to only a ten-fold reduction of bacterial counts compared to wild-type). As expected, functional complementation (*i.e.*, introduction of a plasmid-born wild-type *iglB* allele into the $\Delta iglB$ mutant strain (CpWT) restored wild-type growth.

To confirm that a late phagosomal escape had occurred in the Y139F mutant, we next compared the ability of the $\Delta iglB$ mutants to escape from the phagosomal compartment to that of the wild-type strain, by monitoring co-localization of intracellular bacteria with the phagosomal marker LAMP-1, (**Fig. 5B**) up to 10h after infection in J774-1 macrophages. Colocalization of the wild-type strain with LAMP-1 was below 20% as soon as 1 h after infection. In contrast, the frequency of bacteria co-localizing with LAMP-1 remained elevated (between 60% and 90%), with $\Delta iglB$ (as expected), but also with Y139A and Y139F. In agreement with the kinetics data, this assay confirmed that whereas the wild-type strain had already escaped into the host cell cytosol at 1 h, the Y139A and Y139F mutants were still trapped in the phagosomal compartment at 10 h.

Transmission electron microscopy confirmed that a clear cytosolic multiplication was visible at 24 h with the Y139F mutant but not with the Y139A mutant (**Fig. 6A**), fully supporting the kinetics and confocal data (Fig 5A). We therefore next used time-lapse video microscopy to visualize in real time multiplication of the Y139F mutant in J774-1 macrophages. For this, we

inserted a GFP-encoding gene into plasmids pKK214::pGro ig /B and pKK214::pGro ig /BY139F (yielding recombinant plasmids pKK214::pGro ig /B-pGro gfp and pKK214::pGro ig /BY139F-pGro gfp , respectively). *F. novicida* Δig /B was transformed with these GFP-expressing recombinant plasmids. We generated J774-1 cells with red nuclei by transduction with NucLight Red Lentivirus to facilitate cell recognition and counting (see Materials and Methods). J774-1 cells with red nuclei were infected by GFP-expressing bacteria at an MOI of 1,000. Infection was followed over a 24h-period, using a fully automated microscope Incucyte® 531 S3 (Essen BioScience). Images were taken every 20 minutes with the 20X objective during 24 h, starting 1 h after infection (**Fig. 6B**; **Videos S1, S2**).

Hence, in perfect agreement with the kinetics and electron microscopy data, time-lapse video microscopy confirmed that, in spite of an initial delay in bacterial multiplication due to altered phagosomal escape (up to 10 h of infection), the Y139F mutant was capable of active cytosolic multiplication at later time points. Hence, it is likely that the Y139F substitution allows the production of sufficient assembled T6SS to promote bacterial phagosomal escape and cytosolic multiplication in these cells.

We also replaced Tyr139 by two phosphomimetics *i.e.* the negatively charged amino acids Aspartate and Glutamate and evaluated the impact of these amino acid substitutions (Y139D and Y139E) on intracellular multiplication in J774-1 cells (**Fig. S6A**). The two mutants led to severe defects in intracellular multiplication and, at all time points tested, the replication defect was comparable to that of the Y139A or ΔFPI mutant. We next evaluated the capacity of the Y139D and Y139E mutants to form sheath-like structure by using the sucrose gradient assay. In the two mutants, the IgB protein was exclusively detected by Western blot in the upper fractions of the sucrose gradient (**Fig. S6B**). These data strongly suggest that residues possibly mimicking the phosphorylated state of Y139 also prevented sheath-like assembly.

Functional assays in primary cultures

Finally, we evaluated the ability of Y139A and Y139F mutants to multiply in primary bone marrow-derived macrophages (BMMs) over a 24 h-period. In these cells, growth of both Y139A and Y139F mutants was similar to that of ΔFPI and Δig /B mutant strains (**Fig. S7A**)

even at 24 h. The ability of the Y139A and Y139F mutants to induce phagosomal membrane rupture in BMMs was also tested using the E-lactamase/CCF4 assay (35, 48). Strains expressing wild-type IgIB showed similar amount of cleaved CCF4 at all time-points tested whereas there was no (or marginal) loss of FRET signal with Δ igIB, Y139A, Y139F, and the two negative control strains, confirming that the Y139A, Y139F mutant strains remained stuck in intact phagosomes during at least the first 6h hours of infection also in these cells (Fig. S7B).

DISCUSSION

This is the first report of protein phosphorylation events in *Francisella*. Our proteomic approaches allowed the identification of a unique residue of the T6SS sheath that is phosphorylated and that plays a critical in phagosomal escape of this pathogenic bacterium.

Pivotal role of tyrosine 139 of IgIB in sheath assembly

Formation of the *Francisella* T6SS is believed to occur in the phagosome before the escape of the bacterium in the cytosol. Once in the cytosol, the T6SS seems to be dispensable for cytosolic multiplication. Nevertheless, some T6SS elements are likely to be required during the cytosolic stage of the infectious cycle. Indeed, most FPI genes are induced during late intra-macrophage growth (49) and IgIC has been shown to be required for intracellular growth of *F. novicida* that are microinjected directly into the cytosol of HeLa cells (21). IgIC secretion in *F. novicida* depends on the T6SS core components IgIA and IgIB (50). Of note, truncated IgIA proteins still able to form IgIA/IgIB-heterodimers have been reported to have lost their IgIC secretory function (26), suggesting that heterodimer formation is not sufficient to generate a functional sheath.

We showed that the single substitution of IgIB residue 139 either by alanine, aspartate or glutamate (Y139A, Y139D or Y139E) was sufficient to abrogate T6SS assembly, prevent phagosomal escape and abolish intracellular bacterial multiplication. Of note, these three amino acid substitutions eliminate the phenol ring. In contrast, the substitution Y139F, which

preserves the phenol ring but not the phosphorylatable OH moiety, could still assemble possibly unstable sheath-like structure (**Fig. 4D, E**) and allow bacterial multiplication in J7741 macrophages (**Fig. 5A; Fig. 6A, B; video S2**). Indeed, the kinetics of intracellular multiplication, the electron microscopy and time-lapse video microscopy assays all confirmed that, in spite of an altered phagosomal escape, the Y139F mutant was able to access the cytosolic compartment and promote active multiplication in this compartment.

Of note, we found that multiplication of the Y139F was abrogated in primary bone marrow-derived macrophages, probably due to the high bactericidal activity of these cells. Altogether these data support the notions that: i) both the phenol ring steric hindrance and the OH moiety are key to T6SS assembly; and ii) the phosphorylation of OH on the Y139 is not favorable to sheath polymerization. At this stage, the inability of the Y139F mutant to form stable T6SS might be explained by the fact that it maintains the phenol rings but it lacks the OH moiety. Of note, it was demonstrated that a single tyrosine Hydroxyl Group controlled the specificity of *Plasmodium falciparum* ferredoxin-NADP⁺ reductase (51).

Although inspection of the 3.7 Å EM reconstruction of the *F. novicida* contracted sheath (PDB 3j9o) does not show any atoms close enough to form a hydrogen bond with the hydroxyl of Y139, the carboxylates of D114 from IgIB, and D63 of IgIA in the next dimer, are around 5 Å away and these may approach close enough to Y139 OH to form hydrogen bond interactions stabilizing the assembly. 3D modeling also indicated that there is space for a phosphate group on this atom as the OH is pointing into a pocket in the structure (**Fig. 3**).

However, the negatively charged phosphate would induce charge repulsion with the nearby Asps from the next dimer most likely preventing assembly of the strands when Y139 is phosphorylated. Hence, the charge repulsion provoked by addition of the phosphorylation moiety (when Y139 is phosphorylated) is likely to weaken the stability of the contracted sheath. Altogether these data suggest that the phosphorylation status of IgIB could modulate T6SS assembly/disassembly process. Supporting the notion that phosphorylation of Y139 impairs sheath contraction, replacement of this residue by a phosphomimetic (Y139D or

Y139E) led to a severe intracellular multiplication defect and prevented sheath-like structure formation.

IglB phosphorylation, a new mediator of T6SS dissociation?

The assembly of the T6SS-H1 of *Pseudomonas aeruginosa* has been shown to be spatially regulated by a post-translational mechanism coined « the Threonine Protein Phosphorylation » (or TPP) Pathway. During this process, involved in the defense of bacteria to a neighboring attack, a membrane-bound threonine kinase phosphorylates a forkhead-associated domain-containing Protein (FhA or TagH), which promotes the assembly of an active conformation of the T6SS at the site of the attack (52-54). Recently, the offensive antibacterial T6SS of *Serratia marcescens* has also been shown to be controlled by the opposing actions of the TPP pathway and TagF on assembly of the core machinery (55). The TPP represents the only currently identified post-translational mechanism regulating T6SS biogenesis. Since the *Francisella* genomes do not encode any putative tyrosine kinase, yet unidentified protein(s) with a non-canonical tyrosine kinase activity may be responsible for IglB phosphorylation.

In contrast to all the canonical T6SS, the FPI does not encode any homologue of the unfoldase ClpV, but instead uses the general chaperone ClpB for the recycling of the contracted sheaths. Indeed, Basler and co-workers have recently shown that *F. novicida* assembled its T6SS sheath on the bacterial poles and that the sheath cycled through assembly, contraction and disassembly, similarly to what was previously described for other canonical T6SSs (7). ClpB was shown to specifically localize with the contracted sheaths and is responsible for their disassembly within phagosomes of infected macrophages. Interestingly, the amounts of ClpB were not (or marginally) up-regulated upon KCl induction

(i.e. only 1.3-fold more ClpB in KCl-induced conditions compared to non-induced conditions).

ClpB was also mainly associated with the soluble fraction of the sucrose gradient of KCl-induced bacteria). IglB phosphorylation might assist ClpB when the sheath is contracted to promote its dissociation (**Fig. 7**). The kinase activity leading to IglB phosphorylation might

assemble, like ClpB, at the pole of the bacterium only when the sheath is contracted and assist sheath dissociation. However, our careful inspection of the *Francisella* genomes did not identify any gene encoding for a putative serine/threonine- or tyrosine-kinase.

Of note, two proteins, FTN_0459, predicted to encode a UbiB kinase, and the histidine kinase kdpD, were found to be phosphorylated (on T128, T165/S166, S176 and T173 for UbiB and on S670 for KdpD; Table S4). The UbiB protein family is a widespread family of kinase-like present in the three kingdoms of life, often required for the biosynthesis of isoprenoid lipids. In *Escherichia coli*, UbiB has been shown to be required for the aerobic biosynthesis of the redox-active lipid ubiquinone, coenzyme Q (56). It has been assumed but not formally established that UbiB family members were protein kinases. Two-component systems (TCS) are known to be involved in multiple physiological responses and the regulation of virulence in many bacteria. These signal transduction systems involve two proteins: a sensing protein and a transcription factor. The membrane sensor is a histidine kinase that mediates phosphotransfer to a DNA-binding regulatory protein with a phosphorylated aspartate phosphoacceptor site that alter the level of gene expression. *F. novicida* has two complete TCS, including KdpD (the histidine kinase FTN_1715) / KdpE (the regulatory protein FTN_1714) (57). KdpD, whose predicted phosphorylation site is Histidine 674, has been also shown to be responsible for the phosphorylation of protein FTN_1465 (also designated QseB or PmrA) at the aspartic acid at position

51, suggesting the existence of possible crosstalks between complete and incomplete TCS in *Francisella*. However, possible correlations between such kinases and tyrosine phosphorylation remain purely speculative.

This suggests that a yet unidentified enzyme with either a non-canonical tyrosine kinase activity or a protein predicted to be involved in a different enzymatic reaction with a « moonlight » tyrosine kinase activity, is responsible for IgIB phosphorylation. If so, its identification might prove extremely difficult and would require extensive future work. It is also possible that a single kinase mutant might have no or very limited effect on phagosomal disruption since sheath polymerization would occur and be sufficient to promote phagosomal membrane disruption. Indeed, it has been shown (21) that only a minor fraction of functional T6SS is sufficient to promote phagosomal escape and, once in the cytosol, FPI mutants can multiply like wild-type bacteria.

In bacteria such as *Escherichia coli*, *Vibrio cholerae* or *Pseudomonas aeruginosa*, the sheath contracts spontaneously during the repeated rounds of ultraspeed purification required for their isolation from cell cultures (58). In *Francisella*, T6SS contraction can be triggered in culture either by placement under coverslips or by KCl stimulation (26). We found in this study that the amounts of more than two hundred proteins were altered upon KCl stimulation (**Fig. 1**). Hence, proteins that were upregulated upon KCL stimulation might also contribute to T6SS biogenesis (such as proteins involved in Iron-sulfur clusters biogenesis or in iron acquisition). Notably, the down-regulated proteins comprized seven proteins (FTN_0042 - FTN_0048) out of the 13 proteins potentially encoded by the *Francisella novicida* island (FNI, FTN_0042 - FTN_0054) (35). Although inactivation of the whole FNI locus had no effect on *F. novivcida* virulence, a possible contribution of the orthologues of IglA and IglB (FTN_0042 and FTN_0043) to the sheath assembly-disassembly process cannot be excluded.

In conclusion, our mass spectrometry analyses revealed that the sheath protein IglB was the only T6SS component to contain a phosphorylatable residue (Y139). Importantly, our functional assays demonstrated that Y139 played a critical role in functional T6SS assembly.

Acknowledgements

We thank Dr A. Sjöstedt for providing the *F. novicida* strain U112 and Alain Schmitt (Cochin Institute Electron Microscopy Facility) for excellent technical support. These studies were supported by INSERM, CNRS and Université Paris Descartes Paris Cité Sorbonne. Jason Ziveri was funded by a fellowship from the “Délégation Générale à l’Armement”. Claire Lays was funded by a fellowship from the LABEX ECOFECT (ANR-11-LABX-0048) of Université de Lyon, within the program "Investissement d’Avenir" (ANR-11-IDEX-0007) operated by the French National Research Agency (ANR).

References

1. Sjostedt, A. (2007) Tularemia: history, epidemiology, pathogen physiology, and clinical manifestations. *Ann N Y Acad Sci* 1105, 1-29
2. Sjostedt, A., ed. (2011) *Francisella tularensis and tularemia*, Fontiers Media SA
3. Luque-Larena, J. J., Mougeot, F., Arroyo, B., Vidal, M. D., Rodriguez-Pastor, R., Escudero, R., Anda, P., and Lambin, X. (2017) Irruptive mammal host populations shape tularemia epidemiology. *PLoS Pathog* 13, e1006622
4. Maurin, M., and Gyuranecz, M. (2016) Tularaemia: clinical aspects in Europe. *Lancet Infect Dis* 16, 113-124
5. McLendon, M. K., Apicella, M. A., and Allen, L. A. (2006) Francisella tularensis: taxonomy, genetics, and Immunopathogenesis of a potential agent of biowarfare. *Annu Rev Microbiol* 60, 167-185
6. Kingry, L. C., and Petersen, J. M. (2014) Comparative review of Francisella tularensis and Francisella novicida. *Front Cell Infect Microbiol* 4, 35
7. Brodmann, M., Dreier, R. F., Broz, P., and Basler, M. (2017) Francisella requires dynamic type VI secretion system and ClpB to deliver effectors for phagosomal escape. *Nat Commun* 8, 15853
8. Eshraghi, A., Kim, J., Walls, A. C., Ledvina, H. E., Miller, C. N., Ramsey, K. M., Whitney, J. C., Radey, M. C., Peterson, S. B., Ruhland, B. R., Tran, B. Q., Goo, Y. A., Goodlett, D. R., Dove, S. L., Celli, J., Veessler, D., and Mougous, J. D. (2016) Secreted Effectors Encoded within and outside of the Francisella Pathogenicity Island Promote Intramacrophage Growth. *Cell Host Microbe* 20, 573-583
9. Lagrange, B., Benaoudia, S., Wallet, P., Magnotti, F., Provost, A., Michal, F., Martin, A., Di Lorenzo, F., Py, B. F., Molinaro, A., and Henry, T. (2018) Human caspase-4 detects tetra-acylated LPS and cytosolic Francisella and functions differently from murine caspase-11. *Nat Commun* 9, 242

10. Santic, M., Molmeret, M., Klose, K. E., and Abu Kwaik, Y. (2006) *Francisella tularensis* travels a novel, twisted road within macrophages. *Trends Microbiol* 14, 37-44
11. Pizarro-Cerda, J., Charbit, A., Enninga, J., Lafont, F., and Cossart, P. (2016) Manipulation of host membranes by the bacterial pathogens *Listeria*, *Francisella*, *Shigella* and *Yersinia*. *Semin Cell Dev Biol*
12. Charity, J. C., Blalock, L. T., Costante-Hamm, M. M., Kasper, D. L., and Dove, S. L. (2009) Small molecule control of virulence gene expression in *Francisella tularensis*. *PLoS Pathog* 5, e1000641
13. Meibom, K. L., Barel, M., and Charbit, A. (2009) Loops and networks in control of *Francisella tularensis* virulence. *Future Microbiol* 4, 713-729
14. Celli, J., and Zahrt, T. C. (2013) Mechanisms of *Francisella tularensis* intracellular pathogenesis. *Cold Spring Harb Perspect Med* 3, a010314
15. Ramsey, K. M., Osborne, M. L., Vvedenskaya, I. O., Su, C., Nickels, B. E., and Dove, S. L. (2015) Ubiquitous promoter-localization of essential virulence regulators in *Francisella tularensis*. *PLoS Pathog* 11, e1004793
16. Ziveri, J., Barel, M., and Charbit, A. (2017) Importance of Metabolic Adaptations in *Francisella* Pathogenesis. *Front Cell Infect Microbiol* 7, 96
17. Bröms, J. E., Sjöstedt, A., and Lavander, M. (2010) The Role of the *Francisella Tularensis* Pathogenicity Island in Type VI Secretion, Intracellular Survival, and Modulation of Host Cell Signaling. *Front. Microbiol.* 1, 136.
18. Clemens, D. L., Lee, B. Y., and Horwitz, M. A. (2018) The *Francisella* Type VI Secretion System. *Front Cell Infect Microbiol* 8, 121
19. Nano, F. E., Zhang, N., Cowley, S. C., Klose, K. E., Cheung, K. K., Roberts, M. J., Ludu, J. S., Letendre, G. W., Meierovics, A. I., Stephens, G., and Elkins, K. L. (2004) A *Francisella tularensis* pathogenicity island required for intramacrophage growth. *J Bacteriol* 186, 6430-6436

20. Lauriano, C. M., Barker, J. R., Yoon, S. S., Nano, F. E., Arulanandam, B. P., Hassett, D. J., and Klose, K. E. (2004) MglA regulates transcription of virulence factors necessary for *Francisella tularensis* intraamoebae and intramacrophage survival. *Proc Natl Acad Sci U S A* 101, 4246-4249
21. Meyer, L., Broms, J. E., Liu, X., Rottenberg, M. E., and Sjostedt, A. (2015) Microinjection of *Francisella tularensis* and *Listeria monocytogenes* reveals the importance of bacterial and host factors for successful replication. *Infect Immun* 83, 3233-3242
22. Cuthbert, B. J., Ross, W., Rohlfing, A. E., Dove, S. L., Gourse, R. L., Brennan, R. G., and Schumacher, M. A. (2017) Dissection of the molecular circuitry controlling virulence in *Francisella tularensis*. *Genes Dev* 31, 1549-1560
23. Russell, A. B., Wexler, A. G., Harding, B. N., Whitney, J. C., Bohn, A. J., Goo, Y. A., Tran, B. Q., Barry, N. A., Zheng, H., Peterson, S. B., Chou, S., Gonen, T., Goodlett, D. R., Goodman, A. L., and Mougous, J. D. (2014) A type VI secretion-related pathway in *Bacteroidetes* mediates interbacterial antagonism. *Cell Host Microbe* 16, 227-236
24. Abby, S. S., Cury, J., Guglielmini, J., Neron, B., Touchon, M., and Rocha, E. P. (2016) Identification of protein secretion systems in bacterial genomes. *Sci Rep* 6, 23080
25. Ledvina, H. E., Kelly, K. A., Eshraghi, A., Plemel, R. L., Peterson, S. B., Lee, B., Steele, S., Adler, M., Kawula, T. H., Merz, A. J., Skerrett, S. J., Celli, J., and Mougous, J. D. (2018) A Phosphatidylinositol 3-Kinase Effector Alters Phagosomal Maturation to Promote Intracellular Growth of *Francisella*. *Cell Host Microbe* 24, 285-295 e288
26. Clemens, D. L., Ge, P., Lee, B. Y., Horwitz, M. A., and Zhou, Z. H. (2015) Atomic structure of T6SS reveals interlaced array essential to function. *Cell* 160, 940-951

27. Nazarov, S., Schneider, J. P., Brackmann, M., Goldie, K. N., Stahlberg, H., and Basler, M. (2018) Cryo-EM reconstruction of Type VI secretion system baseplate and sheath distal end. *EMBO J* 37
28. Vettiger, A., and Basler, M. (2016) Type VI Secretion System Substrates Are Transferred and Reused among Sister Cells. *Cell* 167, 99-110 e112
29. Chamberlain, R. E. (1965) Evaluation of Live Tularemia Vaccine Prepared in a Chemically Defined Medium. *Appl Microbiol* 13, 232-235
30. Gesbert, G., Ramond, E., Tros, F., Dairou, J., Frapy, E., Barel, M., and Charbit, A. (2015) Importance of branched-chain amino acid utilization in *Francisella* intracellular adaptation. *Infect Immun* 83, 173-183
31. Lipecka, J., Chhuon, C., Bourderioux, M., Bessard, M. A., van Endert, P., Edelman, A., and Guerrera, I. C. (2016) Sensitivity of mass spectrometry analysis depends on the shape of the filtration unit used for filter aided sample preparation (FASP). *Proteomics* 16, 1852-1857
32. Cox, J., and Mann, M. (2008) MaxQuant enables high peptide identification rates, individualized p.p.b.-range mass accuracies and proteome-wide protein quantification. *Nat Biotechnol* 26, 1367-1372
33. Abd, H., Johansson, T., Golovliov, I., Sandstrom, G., and Forsman, M. (2003) Survival and growth of *Francisella tularensis* in *Acanthamoeba castellanii*. *Appl Environ Microbiol* 69, 600-606
34. Ziveri, J., Tros, F., Guerrera, I. C., Chhuon, C., Audry, M., Dupuis, M., Barel, M., Korniotis, S., Fillatreau, S., Gales, L., Cahoreau, E., and Charbit, A. (2017) The metabolic enzyme fructose-1,6-bisphosphate aldolase acts as a transcriptional regulator in pathogenic *Francisella*. *Nat Commun* 8, 853
35. Rigard, M., Boms, J. E., Mosnier, A., Hologne, M., Martin, A., Lindgren, L., Punginelli, C., Lays, C., Walker, O., Charbit, A., Telouk, P., Conlan, W., Terradot, L., Sjostedt, A., and Henry, T. (2016) *Francisella tularensis* IgG Belongs to a Novel

- Family of PAAR-Like T6SS Proteins and Harbors a Unique N-terminal Extension Required for Virulence. *PLoS Pathog* 12, e1005821
36. Meunier, E., Wallet, P., Dreier, R. F., Costanzo, S., Anton, L., Ruhl, S., Dussurgey, S., Dick, M. S., Kistner, A., Rigard, M., Degrandi, D., Pfeffer, K., Yamamoto, M., Henry, T., and Broz, P. (2015) Guanylate-binding proteins promote activation of the AIM2 inflammasome during infection with *Francisella novicida*. *Nat Immunol* 16, 476-484
 37. Edgar, R. C. (2004) MUSCLE: a multiple sequence alignment method with reduced time and space complexity. *BMC Bioinformatics* 5, 113
 38. Fu, A. Q., Genereux, D. P., Stoger, R., Burden, A. F., Laird, C. D., and Stephens, M. (2012) Statistical inference of in vivo properties of human DNA methyltransferases from double-stranded methylation patterns. *PLoS One* 7, e32225
 39. Robert, X., and Gouet, P. (2014) Deciphering key features in protein structures with the new ENDscript server. *Nucleic Acids Res* 42, W320-324
 40. Perez-Riverol, Y., Xu, Q. W., Wang, R., Uszkoreit, J., Griss, J., Sanchez, A., Reisinger, F., Csordas, A., Ternent, T., Del-Toro, N., Dianes, J. A., Eisenacher, M., Hermjakob, H., and Vizcaino, J. A. (2016) PRIDE Inspector Toolsuite: Moving Toward a Universal Visualization Tool for Proteomics Data Standard Formats and Quality Assessment of ProteomeXchange Datasets. *Mol Cell Proteomics* 15, 305-317
 41. Sullivan, J. T., Jeffery, E. F., Shannon, J. D., and Ramakrishnan, G. (2006) Characterization of the siderophore of *Francisella tularensis* and role of *fsIA* in siderophore production. *J Bacteriol* 188, 3785-3795
 42. Kiss, K., Liu, W., Huntley, J. F., Norgard, M. V., and Hansen, E. J. (2008) Characterization of *fig* operon mutants of *Francisella novicida* U112. *FEMS Microbiol Lett* 285, 270-277
 43. Roche, B., Aussel, L., Ezraty, B., Mandin, P., Py, B., and Barras, F. (2013) Reprint of:

- Iron/sulfur proteins biogenesis in prokaryotes: formation, regulation and diversity.
Biochim Biophys Acta 1827, 923-937
44. Mettert, E. L., and Kiley, P. J. (2015) Fe-S proteins that regulate gene expression.
Biochim Biophys Acta 1853, 1284-1293
 45. Weiss, D. S., Brotcke, A., Henry, T., Margolis, J. J., Chan, K., and Monack, D. M.
(2007) In vivo negative selection screen identifies genes required for *Francisella*
virulence. *Proc Natl Acad Sci U S A* 104, 6037-6042
 46. Broms, J. E., Lavander, M., and Sjostedt, A. (2009) A conserved alpha-helix essential
for a type VI secretion-like system of *Francisella tularensis*. *J Bacteriol* 191, 2431-
2446
 47. Spidlova, P., and Stulik, J. (2017) *Francisella tularensis* type VI secretion system
comes of age. *Virulence* 8, 628-631
 48. Ramond, E., Gesbert, G., Guerrero, I. C., Chhuon, C., Dupuis, M., Rigard, M., Henry,
T., Barel, M., and Charbit, A. (2015) Importance of host cell arginine uptake in
Francisella phagosomal escape and ribosomal protein amounts. *Mol Cell Proteomics*
14, 870-881
 49. Wehrly, T. D., Chong, A., Virtaneva, K., Sturdevant, D. E., Child, R., Edwards, J. A.,
Brouwer, D., Nair, V., Fischer, E. R., Wicke, L., Curda, A. J., Kupko, J. J., 3rd,
Martens, C., Crane, D. D., Bosio, C. M., Porcella, S. F., and Celli, J. (2009)
Intracellular biology and virulence determinants of *Francisella tularensis* revealed by
transcriptional profiling inside macrophages. *Cell Microbiol* 11, 1128-1150
 50. Ludu, J. S., de Bruin, O. M., Duplantis, B. N., Schmerk, C. L., Chou, A. Y., Elkins, K.
L., and Nano, F. E. (2008) The *Francisella* pathogenicity island protein PdpD is
required for full virulence and associates with homologues of the type VI secretion
system. *J Bacteriol* 190, 4584-4595

51. Baroni, S., Pandini, V., Vanoni, M. A., and Aliverti, A. (2012) A single tyrosine hydroxyl group almost entirely controls the NADPH specificity of *Plasmodium falciparum* ferredoxin-NADP⁺ reductase. *Biochemistry* 51, 3819-3826
52. Mougous, J. D., Gifford, C. A., Ramsdell, T. L., and Mekalanos, J. J. (2007) Threonine phosphorylation post-translationally regulates protein secretion in *Pseudomonas aeruginosa*. *Nat Cell Biol* 9, 797-803
53. Silverman, J. M., Brunet, Y. R., Cascales, E., and Mougous, J. D. (2012) Structure and regulation of the type VI secretion system. *Annu Rev Microbiol* 66, 453-472
54. Cianfanelli, F. R., Monlezun, L., and Coulthurst, S. J. (2016) Aim, Load, Fire: The Type VI Secretion System, a Bacterial Nanoweapon. *Trends Microbiol* 24, 51-62
55. Ostrowski, A., Cianfanelli, F. R., Porter, M., Mariano, G., Peltier, J., Wong, J. J., Swedlow, J. R., Trost, M., and Coulthurst, S. J. (2018) Killing with proficiency: Integrated post-translational regulation of an offensive Type VI secretion system. *PLoS Pathog* 14, e1007230
56. Aussel, L., Pierrel, F., Loiseau, L., Lombard, M., Fontecave, M., and Barras, F. (2014) Biosynthesis and physiology of coenzyme Q in bacteria. *Biochim Biophys Acta* 1837, 10041011
57. van Hoek, M. L., Hoang, K. V., and Gunn, J. S. (2019) Two-Component Systems in *Francisella* Species. *Front Cell Infect Microbiol* 9, 198
58. Nguyen, V. S., Douzi, B., Durand, E., Roussel, A., Cascales, E., and Cambillau, C. (2018) Towards a complete structural deciphering of Type VI secretion system. *Curr Opin Struct Biol* 49, 77-84

Legends to Figures and Tables

Fig. 1. KCl stimulation of sheath formation

(A) Sucrose gradient. Lysates of bacteria grown in Schaedler K3 medium in the presence of KCl were laid on top of a discontinuous sucrose gradient 15%-55%/Optiprep 55%. Left panel, composition of the gradient; Right panel, transmission electron microscopy (TEM) of the “heavy” fraction (grey arrow, topping the Optiprep cushion). The assembled sheath-like structure, sedimenting at equilibrium to below 55% sucrose, are rod-shaped particles of variable length (100 - 600 nm). One prototypical sheath-like structure is shown. (B) Western blotting analysis of the different fractions, using anti-IgI (A, B or C) antibodies. The grey arrow corresponds to the fraction topping the Optiprep cushion. (C) The proteome of KCl-stimulated and non-stimulated *F. novicida*. Volcano plot representing the statistical comparison of the protein LFQ intensities of KCl-stimulation vs non-stimulated cells. Inner volcano was established using $S0=0.5$, $FDR=0.01$ (class B proteins) and the outer volcano using $S0=0.5$, $FDR=0.001$ (class A proteins). Proteins belonging to the FPI, the Fe uptake and Fe-S clusters are highlighted in color as indicated.

Fig. 2. The phosphoproteome of *F. novicida*

(A) Histograms of the most represented classes of protein. The values correspond to the number of proteins bearing phosphosites in each category. (B) Distribution of phosphosites according to the modified amino acid (tyrosine, Y; threonine, T and serine, S). (C) Heat map of phosphoproteins altered upon KCl stimulation (Pink to right of the FTN numbers corresponds to proteins with multiple phosphorylation sites). The black arrow is pointing to Y139 of IgIB. (D) IgIB phosphorylation distribution. Intensities (in log2) of the non-phosphorylated (left) and phosphorylated (right) Tyr139-containing peptide in the “heavy” (H) and “light” (L) fractions, respectively. The signal of the phosphopeptide was only detectable after

phosphoenrichment. nd, not detectable.

The phosphopeptide NLY(Phospho)DISSSDFFK fragmentation spectrum is available on MS-Viewer (key lkaqklxwx, scan number 38578).

Fig. 3. Predicted role of Y139 of IgIB in sheath assembly

(A) Overview of the sheath that consists of 12 helical strands based on EM reconstruction at 3.7 Å (PDB 3j9o PDB biological assembly1). The strands are built of IgIA/IgIB dimers. IgIB Tyr139 of the coral IgIB/light blue IgIA dimer lies close to the grey/pink IgIA/B dimer in the same strand. It also lies close to the N-terminal extension of the dark blue IgIA from an adjacent strand. The chain coloring is used in the rest of the panels of this figure. **(B)** Close up of the region of Tyr139. The hydroxyl is pointing into a pocket and not obviously making a Hydrogen bond. However, the carboxylates of Asp114 from IgIB and Asp63 of IgIA in the next dimer are around 5 Å away. At the resolution of the reconstruction side chain density is not well defined and these could in fact be close enough to H bond. **(C)** Surface of the assembly clipped to show Tyr139. There is enough space for a phosphogroup on the Tyr. The two Asps will however be close to the phosphogroup and so there is likely to be charge repulsion impairing the sheath assembly, or weakening the sheath stability, when Y139 is phosphorylated.

Fig. 4. Immunodetection of IgIA, IgIB and IgIC in wild-type and IgIB mutant strains

(A) Western Blots (WB) of whole cell protein extracts. Upper gel: WB with anti-IgIB; lower gel: WB with anti-IgIA. **(B)** Western Blots (WB) with anti-IgIC on bacteria / culture filtrates. Bacteria were grown in Schaedler-K3 supplemented or not with 5% KCl until late log phase and then harvested by centrifugation. Culture supernatants were collected after filtration on

0.2 μ M Millipore filters and concentrated using Amicon 3 kDa membranes. The equivalent of 200 μ g of total protein were loaded onto each well. Upper gel, bacterial cultures grown without KCl; lower gel, bacterial cultures supplemented with 5% KCl. **(C)** Coimmunoprecipitations (Co-IP). Upper gel: IP-anti-IgIA, followed by WB with anti-IgIB; lower gel: IP-anti-IgIB, followed by WB with anti-IgIA. **(D)** WBs of sucrose gradient fractions of the Y139F and Y139A mutant strains. **(E)** Distribution of the intensities (transformed in log 2) of the proteins IgIA and IgIB in the Heavy (H) and light (L) sucrose fraction, in cp WT (Δ igIB complemented with WT IgIB), Y139F and Y139A (Δ igIB complemented with IgIB Y139F and IgIB Y139A, respectively).

Fig. 5. Y139A and Y139F IgIB mutants show impaired intracellular survival in J774-1 macrophages

(A) Intracellular bacterial multiplication of wild-type *F. novicida* (WT, Grey squares), isogenic Δ igIB mutant (Δ igIB, blue triangles) and complemented Δ igIB strain (Cp-WT, grey circles; Y139A, blue square; Y139F, red squares) and the Δ FPI control (black lines), was monitored during 24 h in J774A.1 macrophage cells. The values recorded for Y139F, at 24 h, were significantly different from those of Δ FPI, Δ igIB or Y139A. In both cell types, the values recorded for WT or CpWT, at 10 h and 24 h, were significantly different from those of Δ FPI, Δ igIB, Y139A or Y139F. ** $p < 0.001$ (determined by student's t-test). **(B)** Confocal microscopy of intracellular bacteria with J774-1 infected with wild-type *F. novicida* (WT), Δ igIB or complemented strains and their co-localization with the phagosomal marker LAMP1 observed at 1 h, 4 h and 10 h. Upper part: J774.1 were stained for *F. novicida* (green), LAMP1 (red) and host DNA (blue, DAPI stained). Lower part: analysis was performed with ImageJ software. * $p < 0.01$ (determined by student's t-test).

Fig. 6. Electron microscopy and time lapse video microscopy

(A) Transmission electron microscopy of J774-1 cells infected with Y139F, Y139A or WT *F. novicida* at 24 h. Active bacterial multiplication was visible in the cytosol of both WT- and

Y139F-infected cells (first and third panels show a single cell infected with multiple bacteria). In contrast, only rare bacteria could be visualized with Y139A-infected cells. The middle panel shows one cell infected with a unique bacterium (the black arrowhead points to a single bacterium still entrapped in a vacuolar compartment). **(B)** Time lapse video microscopy. J774-1 cells expressing a nuclear restricted Red Fluorescent Protein were infected with GFP-expressing WT and Y139 IgIB proteins. Representative images were taken at 4, 8 h and 20 h (see Video S1 and S2). Red: cell nuclei. Green: GFP expressing bacteria.

Fig. 7. Model of T6SS dynamics

Schematic depiction of the three major steps of the T6SS dynamics. Proposed contribution of IgIB phosphorylation to T6SS disassembly.

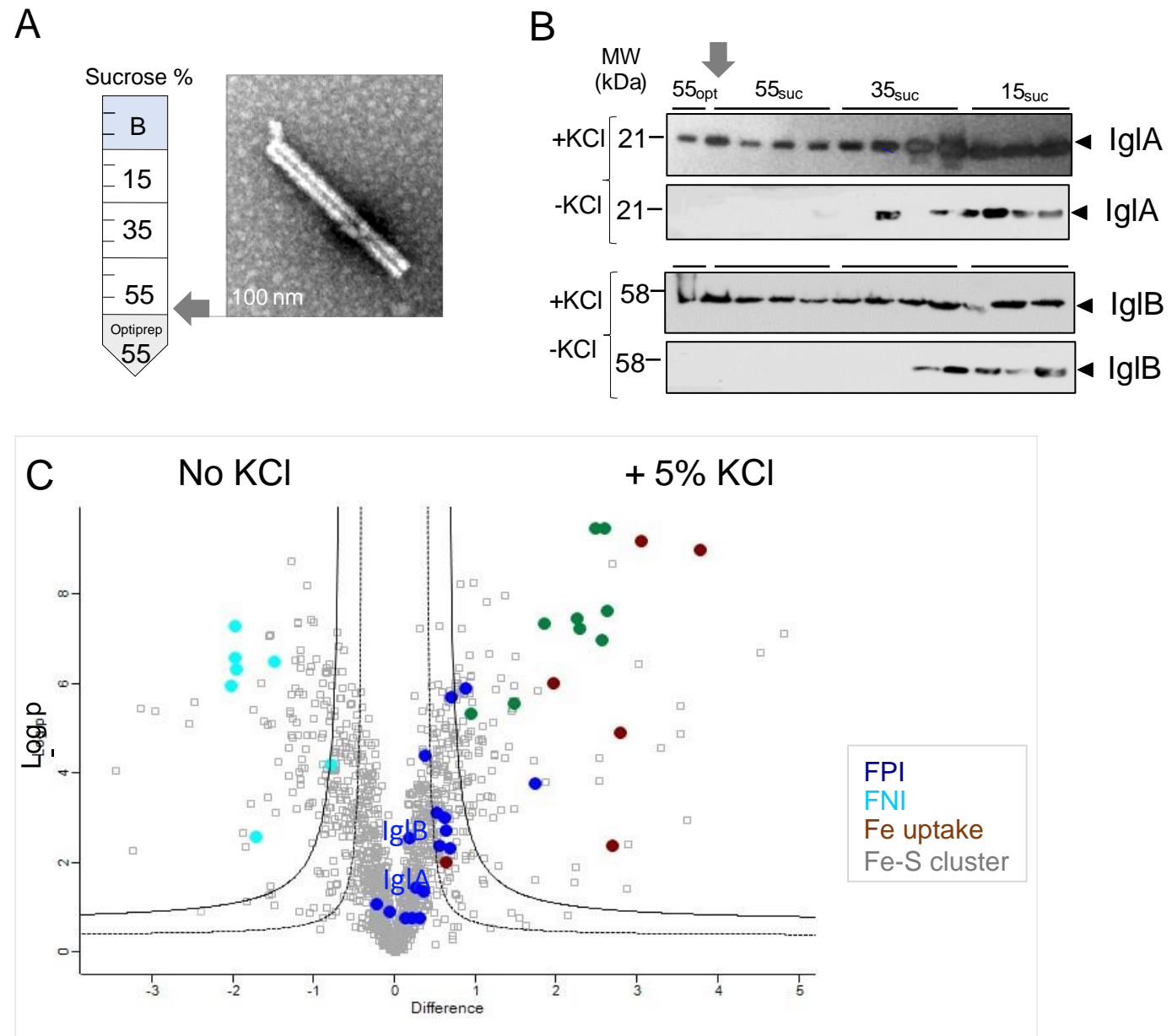
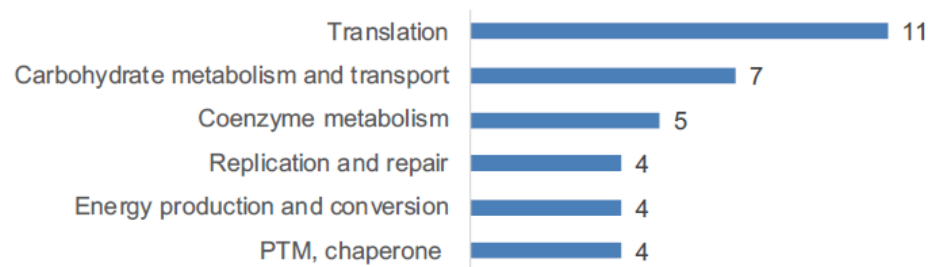


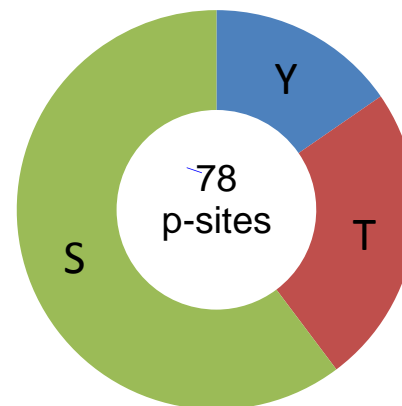
Figure 1. Ziveri et al.

A

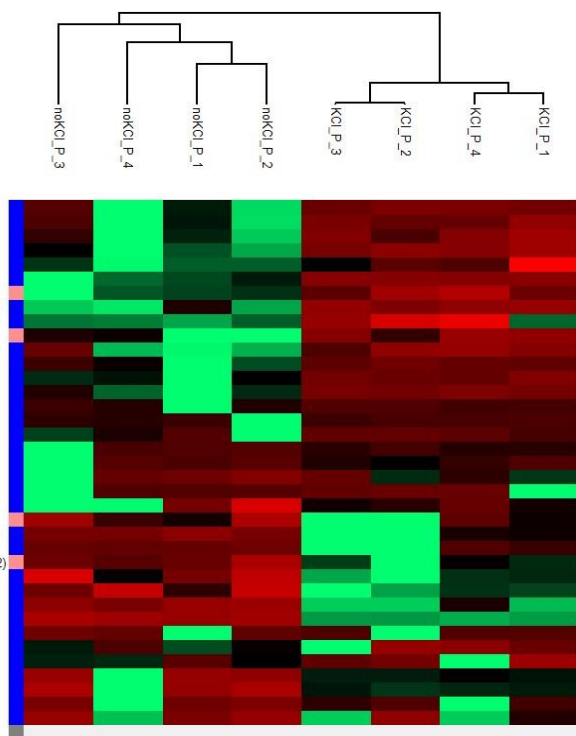
Classes of phosphorylated proteins



B



C



D

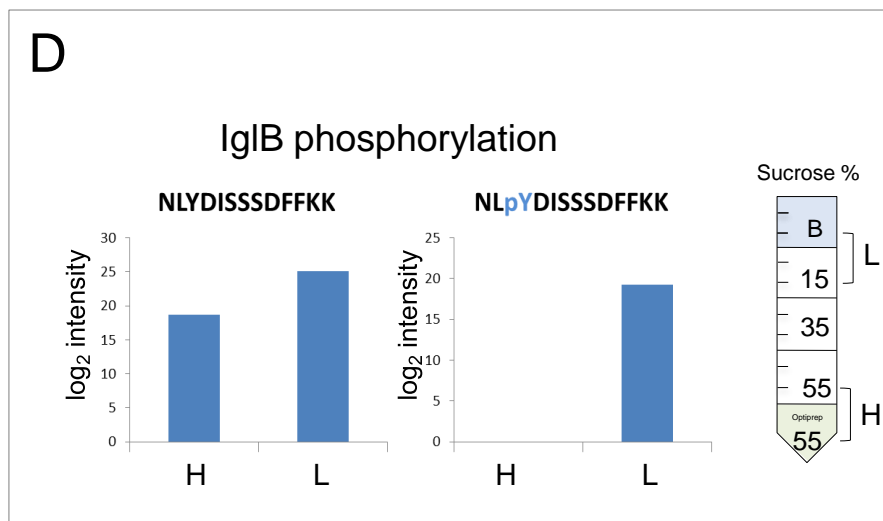


Figure 2 Ziveri et al.

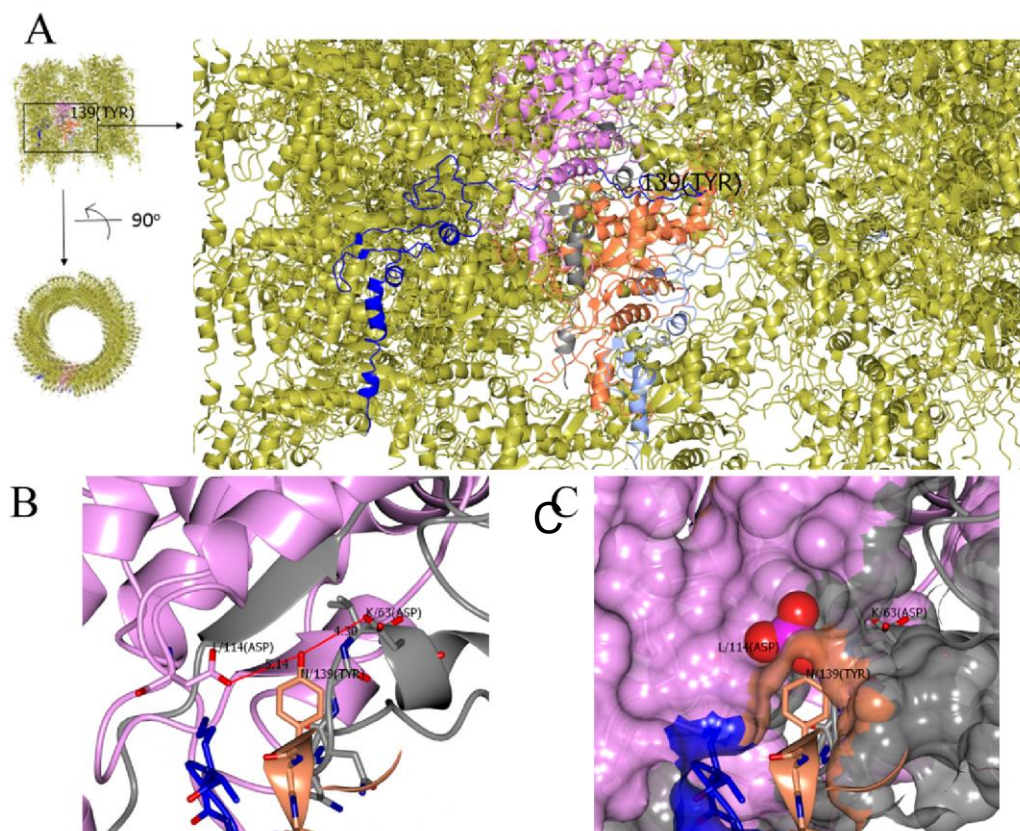


Figure 3. Ziveri et al.

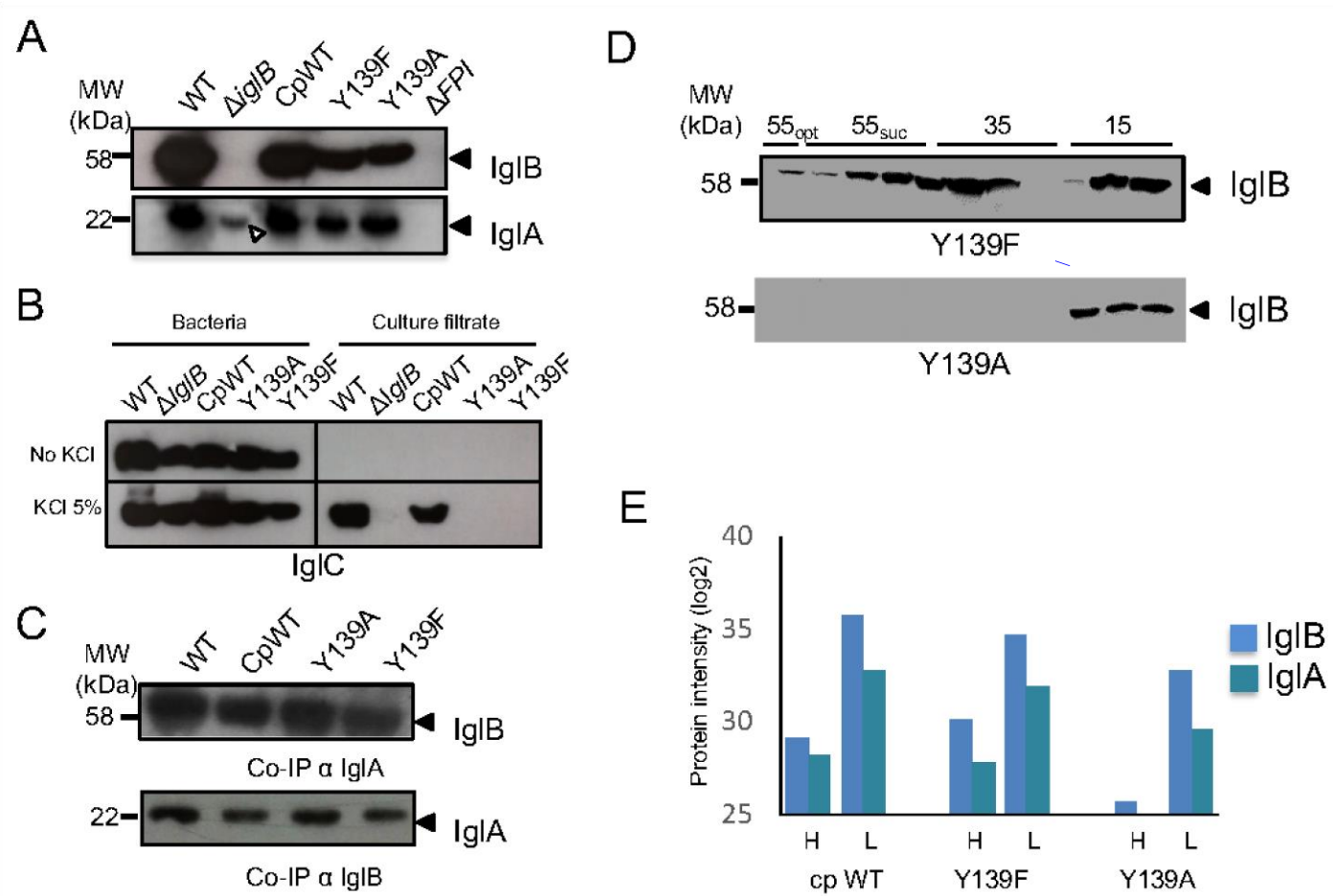
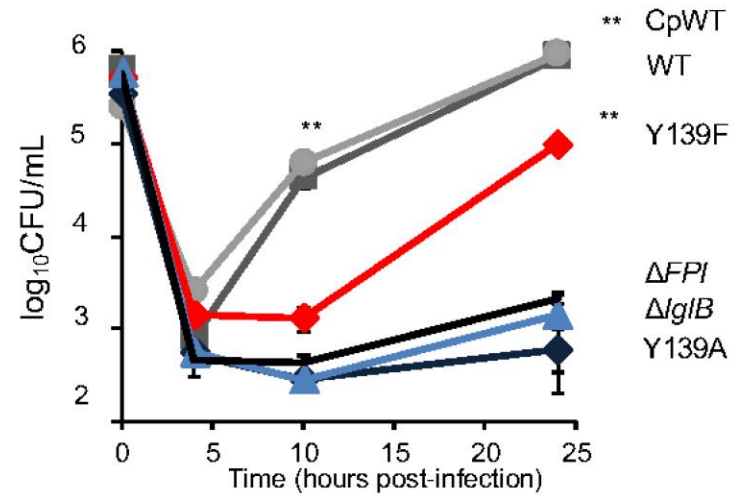


Figure 4. Ziveri et al.

A



B

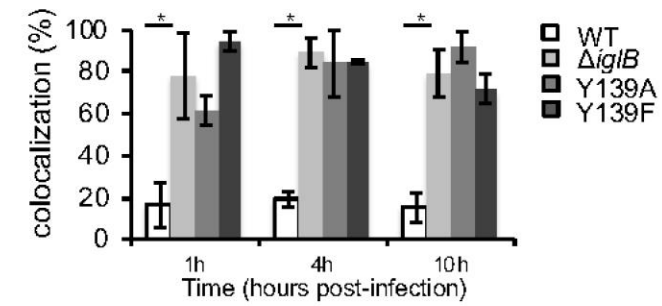
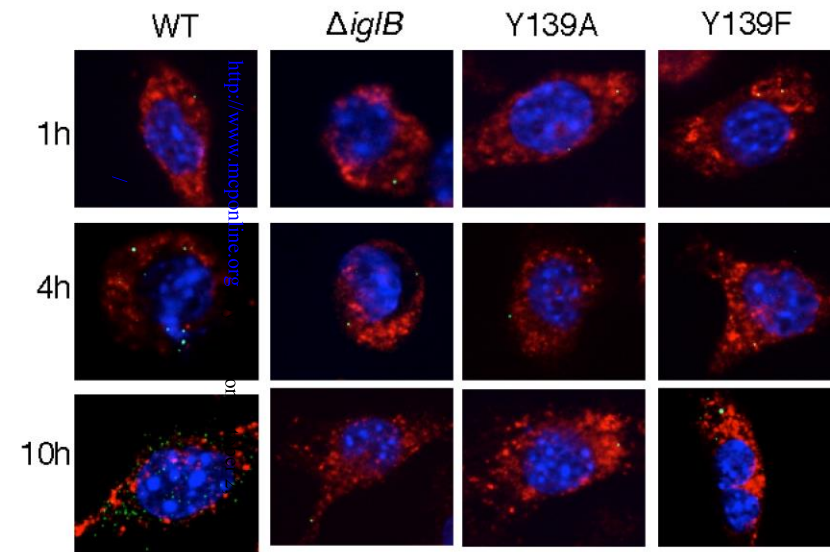


Figure 5. Ziveri et al.

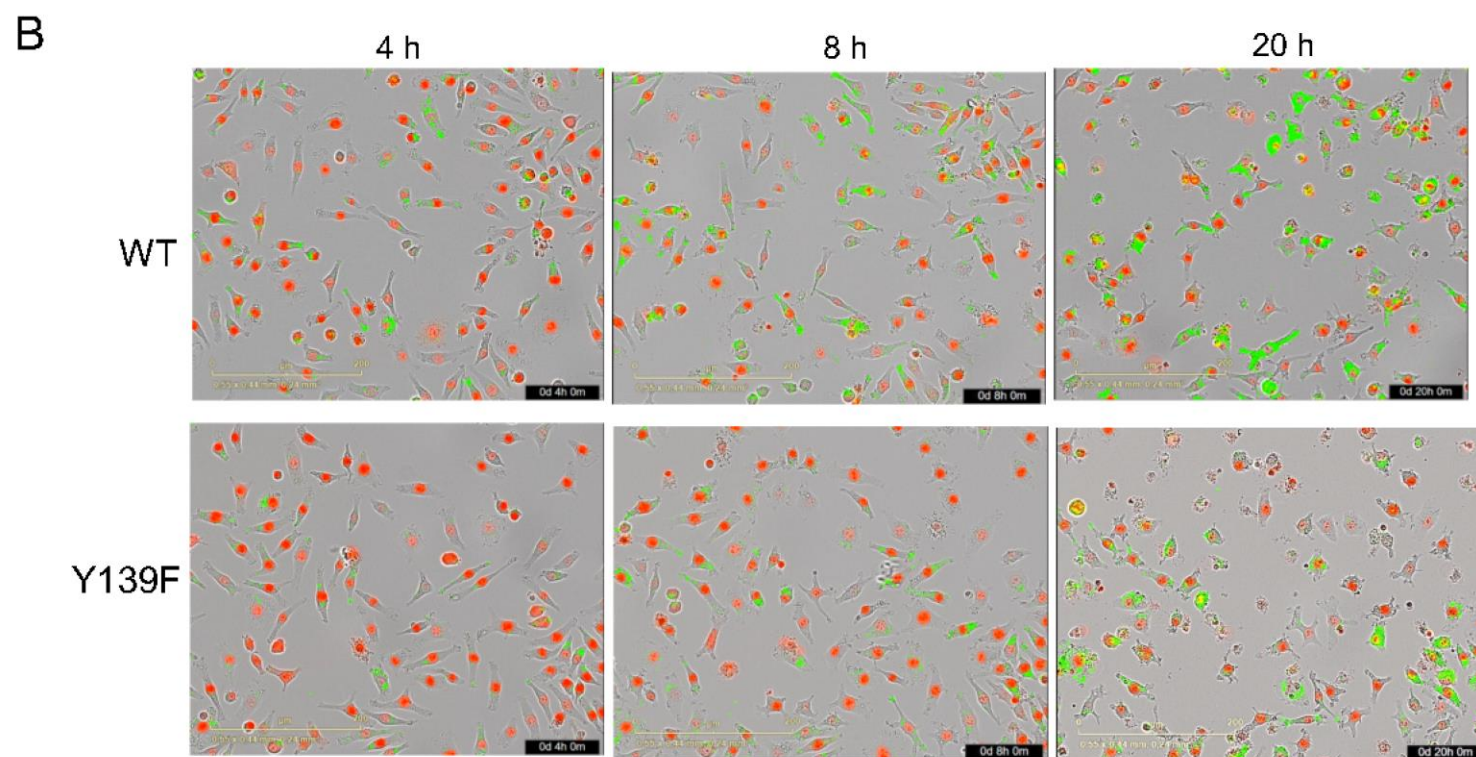
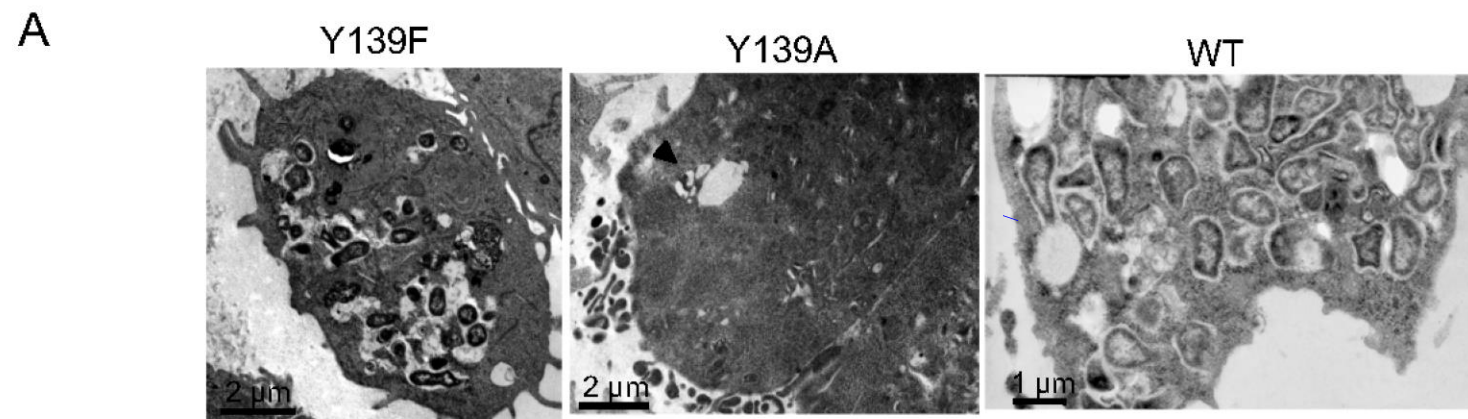


Figure 6. Ziveri et al.

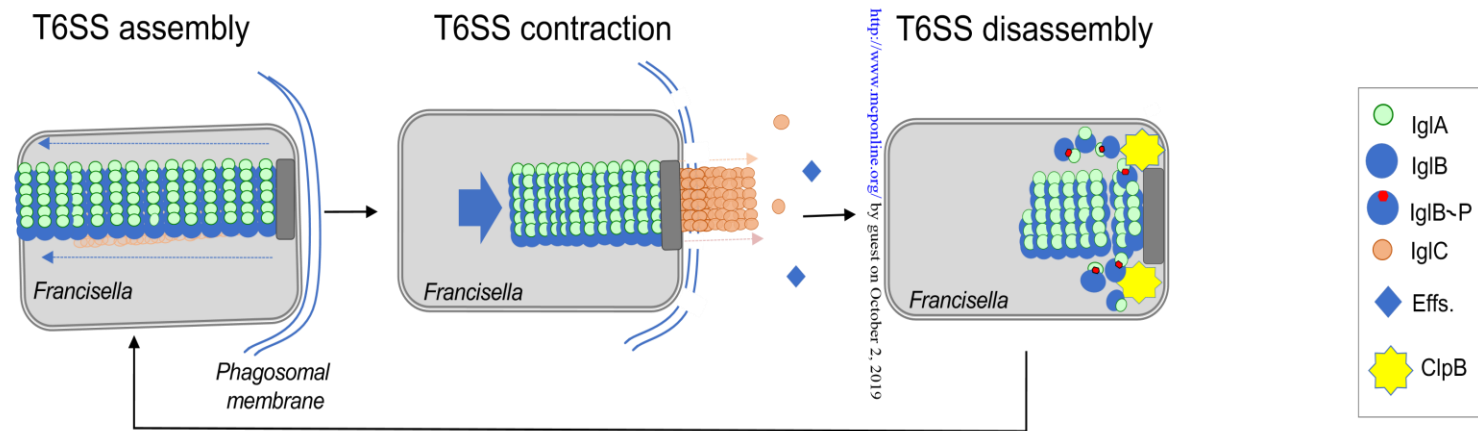


Figure 7. Ziveri et al.